Joint MSC-E/MSC-W Report

EMEP/MSC-E Technical Report 7/2009

July 2009

Development of the EMEP global modelling framework: Progress report

Travnikov O., J.E. Jonson, A.S Andersen, M. Gauss, A. Gusev, O. Rozovskaya, D. Simpson, V. Sokovyh, S. Valiyaveetil and P. Wind

msc-e

Meteorological Synthesizing Centre - East
Krasina pereulok, 16/1
123056 Moscow
Russia

Tel.: +7 495 981 15 66
Fax: +7 495 981 15 67
E-mail: msce@msceast.org
Internet: www.msceast.org

msc-w

Norwegian Meteorological Institute (met.no)
Postboks 43 Blindren
N-01313 Oslo
Norway

Phone: +47 22 96 30 00
Fax: +47 22 96 30 50
E-mail: emep.mscw@met.no
Internet: www.emep.int

CONTENTS

INTRODUCTION

A number of pollutants considered under the LRTAP Convention (hereafter the Convention) exhibits apparent abilities for atmospheric transport over long distances significantly exceeding local or regional scales. They include substances with very long residence time in the atmosphere, like mercury, some persistent organic compounds and to some extent ozone that are dispersed throughout the Northern Hemisphere or even globally. They also include shorter-lived pollutants, like particulate matter, which contribute to episodic intercontinental transport. Thus, pollution levels of these substances in Europe or other regions can be substantially affected by atmospheric transport from other continents. In this aspect, fulfilment of the EMEP task within the Convention to provide information on the pollution levels and origin of these pollutants in the EMEP area requires extension of the modelling activity to the global scale.

Another argument supporting the necessary extension of the EMEP scope is the increased focus of the Convention on Eastern European, Caucasus and Central Asian (EECCA) countries. Support to these countries with full information on transboundary air pollution is one of the priority tasks within EMEP. On the other hand, pollution levels in the Central Asian countries are largely affected by emission sources located outside the EMEP domain (in other Asian countries, like China, India, Pakistan, Iran, etc.) which should be correctly taken into account.

Recognizing the importance of the hemispheric/global scale consideration of air pollution, the Convention established the Task Force on Hemispheric Transport of Air Pollution (TF HTAP). The main focus of the TF HTAP is the determination of the extent and impact of the intercontinental transport of air pollution and to foster international co-operation in this field.

In line with the EMEP priorities, the two EMEP Modelling Centres (MSC-E and MSC-W) have recently extended their modelling capabilities to the global scale. In 2007 the Steering Body to EMEP recommended MSC-W and MSC-E to co-ordinate their efforts developing a common EMEP global modelling system to reduce overlaps of the tasks performed. Appropriate activity was also included in the 2009 EMEP Work-plan [*ECE/EB.AIR/2008/8*]. Besides, the global modelling activity of the EMEP Centres should link and benefit from the work within the TF HTAP.

The first progress in the development of the common EMEP global modelling system was reported last year in the Joint EMEP Centres Progress Report [*Tarrasón and Gusev*, 2008]. The report covers different aspects of MSC-W, MSC-E and CCC activities related to the assessment of air pollution on a global scale. In particular, input information for the global scale modelling (emissions inventories, land cover data, meteorological fields) was compiled and analysed. Particular attention was paid to evaluation of meteorological drivers for the global modelling. Beside, the general concepts and main requirements of a common global modelling system was discussed and formulated. The main requirements include: (1) unified multi-pollutant and (2) multi-media approaches, (3) flexible model domain and resolution, (4) modular structure and (5) computational efficiency. It has been recognized that the proper way to implement these requirements is the development of a modelling *framework* with a flexible modular architecture which could allow constructing a suitable model configuration for a particular pollutant or application task. Besides, the modelling framework should be largely based on parameterizations and approaches already available in the two EMEP Centres to optimize required resources.

This report presents the further progress of the EMEP modelling Centres in the field of the common EMEP global modelling framework. Significant efforts were undertaken for harmonization of input data and modelling approaches applied in the Centres (Chapter 1). Common understanding was achieved for further co-ordinated activities on perspective model development including the grid conventions,

meteorological drivers, land cover and other geophysical information, soil properties data and parameterization of wind re-suspension.

Further improvement of meteorological input for chemical transport modelling on a global scale is discussed in Chapter 2. In particular, the current situation with provision of meteorological input data based on ECMWF/IFS is presented and preliminary results of the WRF model testing are analysed. Chapter 3 contains an overview of recent improvements achieved within the scientific community in the field of anthropogenic emissions inventories on a global scale.

New model developments are outlined in Chapter 4. The model improvements for acidifying pollutants, ozone and PM include steps towards an implementation of convection and convective washout and a model evaluation for Asia. A pilot version of the modelling framework with the modular architecture developed for heavy metals and POPs is presented along with an evaluation of the first modelling results. In addition, implementation of the nesting procedure and development of the multi-media modelling approach for mercury are discussed.

Finally, future activities of the EMEP Centres in the field of global scale modelling are outlined in accordance with the EMEP workplan for 2010.

1. HARMONIZATION OF EXISTING MODELLING APPROACHES AND INPUT DATA

Although there is a clear division of responsibilities between MSC-E and MSC-W there is a number of tasks inherent to model development that are performed at both centres. In this Chapter several such tasks are identified, and measures to minimize the overlap by enhanced co-operation are suggested. Reducing the amount of overlapping tasks and further co-ordination of the two Centres activities in the field of model development will contribute to the fulfilment of the tasks under item 2.4. "Development of integrated EMEP global system" of the 2009 EMEP Work-plan [ECE/EB.AIR/2008/8].

The work on harmonization of the modelling approaches on a global scale was initiated by the Centres last year and first progress in this field was reflected in the Joint EMEP Centres Technical Report [*Tarrasón and Gusev*, 2008]. First of all, the general concepts and major requirements to the global modelling framework was discussed and formulated. Significant attention was also paid to harmonization of input information. In particular, available emissions data required for global scale modelling of different pollutants (including ozone, particulate matter, heavy metals and persistent organic pollutants) were reviewed, different datasets of land cover information were compared and evaluated and two meteorological drivers based on the IFS (ECMWF) and GEM (Environment Canada) weather prediction models were thoroughly tested and evaluated against observations. Besides, the atmospheric dispersion modules of two global models developed in the two Centres were tested within the framework of the TF HTAP tracer experiment (TP1x) along with other chemical transport models.

This year global scale modelling activities of the Centres along with individual work on the further model development and input data improvement include co-ordination efforts on harmonization of modelling approaches made at the Centres technical meeting in St. Petersburg (April, 2009). The main objective of the meeting was to foster the collaboration between scientists involved in the development of global models and to agree on further practical steps towards harmonization of input and output data formats and grid conventions. Major agreements achieved at the meeting are outlined below.

1.1. Grid conventions

Grid conventions are basic characteristics of the model formulation defining requirements to the model input and output data as well as realisation of some model parameterizations. They include type of geographical projection (e.g. lat/long, stereographic, Mercator etc.); spatial coverage and resolution in horizontal; upper boundary, number of layers and type of the co-ordinate system (e.g. pressure, sigma, hybrid co-ordinates) in the vertical.

1.1.1. Horizontal grid

At both centres modelling work is performed using different grid projections. Typical projections are the polar stereographic (as used in the official EMEP model domain) and latitude/longitude grids (typically used in global models). Both models have flexible treatment of coverage and spatial resolution that allows choice of grid size depending on particular task. It was agreed to keep the mentioned above flexibility in the model grid formulation.

In the MSC-W Status Report 1/2008 [*Fagerli et al*., 2008], model result obtained with the Unified EMEP model in several horizontal grid resolutions are compared. The EMEP polar-stereographic grid with 50, 20 and 10 km resolution have been compared. In 2009 a different grid projection (rotated spherical with 20 km resolution) have also been used, showing the full flexibility of the horizontal grid.

To improve the link between different scale simulations with variety of spatial resolutions a nesting procedure is being developed and implemented in the GLEMOS model. In particular, it allows more correct way for setting up boundary conditions for regional modelling and taking into account the effects of the intercontinental transport. The first results and evaluation of the nesting procedure are discussed in Subsection 4.2.3 of this report.

1.1.2. Vertical grid

Current versions of the models have different resolutions and upper boundaries: The Unified EMEP model at MSC-W has an upper boundary at 100 hPa, approximately 12 km. The GLEMOS model at MSC-E has an upper boundary at 10 hPa, approximately 30 km. Both models operate in sigma co-ordinate system, include 20 layers but have different vertical grid structure. Also for the vertical grid further model developments should aim for more flexibility, allowing variable grid resolution and structure depending on the meteorological driver and model applications. Further developments in this direction should be coordinated, satisfying the requirements of both Centres.

1.2. Input data

Significant efforts were undertaken by the Centres at the previous stage [*Tarrasón and Gusev*, 2008] to evaluate different sets of available input data for the global models including meteorological and land cover datasets. Further practical steps will include investigation of the possibility to harmonize input data wherever it is feasible or to unify data formats in order to make an easy exchange and replacement of different sets of input data possible. In particular, new pre-processing and/or reading routines will be coded flexible to allow different options for grid projections and grid resolutions.

1.2.1. Meteorological data

A detailed evaluation of meteorological drivers performed by the Centres [*Tarrasón and Gusev,* 2008] revealed similar satisfactory performance for two meteorological drivers currently in use in the Centres (IFS, GEM). Thus, any of these drivers could be applied by both the Centres in order to harmonize meteorological input. On the other hand, it was realized that availability of a particular meteorological driver for use by each of the Centres is important requirement to the driver.

IFS could be the first candidate for the joint application, since it is widely considered as one of the most advanced meteorological models. According to an agreement between LRTAP convention and ECMWF the EMEP Technical Centres have access to ECMWF archived data on special conditions (the data should not be made available to third parties, and ECMWF should receive reports on the use of the data). The archived IFS data used by MSC-W are originally generated by the University of Oslo re-running the IFS model to get an extended set of out parameters. This set of data is also available for MSC-E. However, availability of IFS for flexible use as a pre-processor is to be further investigated.

In addition, both Centres have started evaluation of the WRF model as a potential candidate for the common meteorological driver. First results of its evaluation on a global scale are presented in Section

2.2. The evaluation of the WRF model should also be regarded as a service for users of the public domain versions of the models.

Along with this, unification of data format and set of meteorological parameters required for modelling activity in both Centres could facilitate harmonization of meteorological input and replaceability of meteorological drivers. Therefore, it was agreed to harmonize the lists of required parameters and other requirements to the data as well as continue discussion on unification of the data formats.

1.2.2. Land cover

Four original sources of land cover information have been evaluated in the previous analysis [*Tarrasón and Gusev,* 2008]. Since no principal advantage of any dataset was identified in the study, harmonisation of the land cover input could be achieved by conventional selection of one of the datasets keeping flexibility of other datasets application as well.

At present the land cover data has to be projected to a specific format and converted into the model grid projection to be used by the model. In the future most of these conversions should be made directly in the model during runtime, using only original raw-data as input. The advantage with this approach is that no changes are needed in the input data when the grid projection is changed. Differences between runs performed in different grids or using different models can then more easily be compared.

1.2.3. Soil properties

Input data on soil properties (soil texture, size distribution, OC content etc.) are of significant interest in both Centres. They are required for parameterization of wind suspension of mineral dust, re-suspension of some pollutants (e.g. heavy metals and POPs) and description of processes in soil. Therefore the co-ordination of the activity between the Centres was discussed on collection, evaluation and processing soil properties data on a global scale.

1.3. Model parameterizations

The Centres also exchanged experience in development and improvement of different model parameterizations applied in the models. Particularly, it was noted that both Centres apply very similar approaches to parameterization of advective transport (Bott advection scheme of the forth order). Therefore, co-ordination of the efforts could significantly facilitate further development of the model advection schemes. It was also suggested to continue collaboration in development of the model wind re-suspension schemes. Significant experience gained in this field could be jointly extended to the global scale.

2. METEOROLOGICAL DATA FOR GLOBAL SCALE MODELLING

This chapter provides an overview of the current status and recent developments in the field of meteorological data support for global scale modelling. For the IFS model a method deriving vertical velocity in the sigma co-ordinates directly from the continuity equation is described. Furthermore preliminary results testing and evaluating the WRF model are presented.

2.1. Provision of meteorological input data based on ECMWF

The IFS (Integrated Forecast System) model system of the European Centre for Medium Range Weather Forecasts (ECMWF, http://www.ecmwf.int) was briefly described in *L.Tarrasón and A.Gusev* [2008] and is comprehensively documented on the web pages of ECMWF (http://www.ecmwf.int/research/ifsdocs/), including all features of the different versions (referred to as 'cycles') of the model system.

IFS is a comprehensive earth-system model system that forms the basis for all data assimilation, forecasting and reanalysis activities at ECMWF and is used to create meteorological input files for the EMEP Unified model.

The IFS is run by the University of Oslo to provide data for all meteorological variables that are relevant for air pollution modelling. The main reason for running the IFS system rather than just using the ECMWF archive (http://www.ecmwf.int/products/data/archive/index.html) is to obtain 3-hourly accumulated convective mass fluxes to be used in the EMEP model for convection. Also, by running IFS the user has full control over which version to use. This allows creating multi-year data sets with the same IFS version, if needed.

The IFS is run with a horizontal resolution of spectral T319, corresponding to about 0.5 degrees horizontal resolution. The model is initialized from assimilated data every 24 hours and run for 36 hours. The first 12 hours are used as spin-up and the following 24 hours are archived. The IFS model generates data on the so-called 'grib' format, a highly compressed, binary data format.

From the grib files, provided by the University of Oslo, MSC-W extracts the variables that are needed in the EMEP Unified model and converts the data into EMEP-readable netCDF or FELT format. This step is followed by the relatively time-consuming transfer from the ECMWF disks located in Reading/UK to a super computing facility in Norway. The interpolation from the Gaussian spectral T319 grid into the EMEP 1ºx1º regular grid and EMEP's 20 layers is done in Norway by MSC-W. A mass filter is applied to ensure mass balance after the interpolation. Table 1 lists the meteorological variables that are extracted from the ECMWF data for the EMEP meteorological input files.

In *L.Tarrasón and A.Gusev* [2008] data for the year 2001, generated with IFS cycle 29r2, were described and compared with the Canadian forecasting and assimilation system GEM. Since then, the IFS model has been run on T319 resolution also for the years 2004 to 2006. IFS cycle 29r2 was used to create the years 2004, 2005, and January to August 2006, while from September 2006 and onwards the IFS cycle 31r1 was used. The conversion from IFS model data to ECMWF meteorological input files has been completed by MSC-W for the year 2006. Data for 2004 and 2005 will be converted when this is needed for scientific studies (e.g. trend studies). It is also considered to run the IFS model on its currently available resolution, which is T799 (~25 km), which would allow the study of local scale atmospheric pollution also with focus on large cities.

Table 1. *Variables included in the EMEP meteorological input files based on ECMWF data (June 2009)*

Component	validity	unit
wind in x direction (u)	instantaneous	m s^{-1}
wind in y direction (v)	instantaneous	m s^{-1}
specific humidity	instantaneous	kg kg^{-1}
sigma dot	at half-levels	s^{-1}
potential temperature	instantaneous	K
precipitation	accumulated	mm (during meteorological timestep, 3 hrs)
3D cloud cover	instantaneous	%
surface pressure	instantaneous	hPa
2m temperature	instantaneous	K
sensible heat flux at surface	averaged	W m^{-2}
latent heat flux at surface	averaged	W m^{-2}
surface stress	averaged	N m^{-2}
convective updraft flux	accumulated	kg m^{-2} (during meteorological timestep, i.e. 3 hrs)
convective downdraft flux	accumulated	kg m^{-2} (during meteorological timestep, i.e. 3 hrs)
convective updraft detrainment	accumulated	kg m^{-2} (during meteorological timestep, i.e. 3 hrs)
convective downdraft detrainment	accumulated	kg m^{-2} (during meteorological timestep, i.e. 3 hrs)
cloud liquid water content	instantaneous	kg kg^{-1}
cloud ice water content	instantaneous	kg kg^{-1}
convective precipitation	accumulated	mm (during meteorological timestep, i.e. 3 hrs)

2.1.1. Calculation of vertical wind velocity in the Unified EMEP model

The vertical wind in the EMEP model is described by sigma dot ($\dot{\sigma}$). It has previously (2001 meteorology) been derived from P dot ($\dot{P}$), which is the corresponding quantity available from IFS. The conversion from $\dot{P}$ in the T319 grid with eta vertical coordinates into the spherical coordinates with sigma levels is a heavy and inaccurate process. This is partly because not all quantities needed for the transformation are accurately known (such as the derivatives of the surface pressure, but also P dot in the spherical projection seems to be rather inaccurate). Sigma dot is subsequently corrected in the mass filtering process.

In the compilation of the 2006 meteorology we have derived sigma dot directly from the continuity equations, avoiding the use of P dot altogether.

The continuity equation in sigma coordinates can be expressed as:

$$(\dot{\sigma})_{k+1/2}\left(P_S - P_{top}\right) = -\frac{\partial P_{k+1/2}}{\partial t} - \sum_{r=k}^{top} \vec{\nabla}\left(\vec{V}_r \Delta P_r\right)$$

Where k is the full level index (k=1 corresponding to top level), k+1/2 is the half level index, P_s is the surface pressure, P_{top} is the pressure at the top of the column, $\vec{\nabla}$ is the horizontal derivative, $\vec{V}$ is the horizontal wind (assumed constant over each vertical layer) and $\Delta P_r = P_{r+1/2} - P_{r-1/2}$.

At surface $(\dot{\sigma})_S = 0$ and $\frac{\partial P_S}{\partial t} = -\sum_{r=S}^{top} \vec{\nabla}\left(\vec{V}_r \Delta P_r\right)$.

Note that this quantity does not depend on σ and can therefore not be changed by correcting σ.

Using the definition of sigma $\left(\sigma = \frac{P - P_{top}}{P_S - P_{top}}\right)$ we get:

$$\frac{\partial P_{k+1/2}}{\partial t} = \frac{\partial P_{k+1/2}}{\partial P_S}\frac{\partial P_S}{\partial t} = \sigma_{k+1/2}\frac{\partial P_S}{\partial t}$$

Combining the three equation gives the following expression for σ:

$$(\sigma)_{k+1/2}\left(P_S - P_{top}\right) = \sigma_{k+1/2}\sum_{r=S}^{top}\vec{\nabla}\left(\vec{V}_r\,\Delta P_r\right) - \sum_{r=k}^{top}\vec{\nabla}\left(\vec{V}_r\,\Delta P_r\right)$$

Use of this formula directly ensures that $(\sigma)_S = 0$ at surface since $\sigma_S = 1$, and $(\sigma)_{top} = 0$ at top since $\sigma_{top} = 0$.

2.2. Preliminary results of the WRF model testing and evaluation

This section is devoted to the discussion of some preliminary results of global-scale testing of the WRF model. A similar evaluation has already been carried out previously by MSC-E and MSC-W for two other meteorological drivers, namely, GEM of Environment Canada and ECMWF IFS [*Tarrasón and Gusev*, 2008].

In this study global simulations of meteorological parameters with WRF have been performed by MSC-E for January and July 2001. The modelling results for air temperature, wind velocity, air moisture, geopotential height and precipitation have been compared with RAOB and GSN measurements and with corresponding results of the GEM model tested at MSC-E earlier. Below a brief description of the WRF model, model set-up and simulation results is presented.

2.2.1. Short description of WRF

The Weather Research and Forecasting (WRF) model [*Michalakes et al.,* 2005; *Skamarock et al.,* 2005] is a next-generation mesoscale numerical weather prediction system designed to serve both operational forecasting and atmospheric research needs (http://www.wrf-model.org/index.php). It is a multi-year project being undertaken by National Center for Atmospheric Research (NCAR) of the USA in collaboration with several agencies.

The following properties of the model seem to be the most important in the context of meteorological preprocessing for air quality modelling: 3-dimensional variational data assimilation system availability; nesting possibility; a wide set of physical parameterizations; different scales (from global to local) and map projections (latitude-longitude, Lambert conformal, polar stereographic, Mercator); system extensibility; computational parallelism opportunity. *A priori* comparison of properties and capabilities of the WRF model and the GEM model tested earlier shows the superiority of WRF in most cases (Table 2, preferable characteristics are marked in bold).

Table 2. *Comparison of WRF and GEM models*

Model properties	WRF	GEM (export version)
Horizontal discretization	Uniform-resolution Aracawa-C	**Variable-resolution Aracawa-C**
Vertical coordinate	Terrain following hydrostatic-pressure	**Hybrid**
Multiscaleness	Yes	Yes
Map projections	**Lat-lon, polar stereographic, Lambert, Mercator**	Lat-lon
Online chemistry model	**Yes (WRF-Chem)**	No
Data assimilation	**Yes**	No
Digital filtering initialization	**Diabatic** **Double (adiabatic backward + diabatic forward)**	Diabatic
User support	**Model website** **Users' workshops** **Tutorials**	Model website

2.2.2. Input data and model settings

Input meteorological analyses data

The testing of WRF was performed on the basis of the ECMWF meteorological analyses

Model grid

WRF model test runs were carried out using the lat-lon grid with horizontal resolution 1°x1°, 20 vertical layers and domain upper boundary at 10hPa.

Calculation cycle

The process of preparation of meteorological data for the long period of time was organized as a sequence of short 36-h runs with 12-h spin-up. 3-dimensional analysis data assimilation was used over the total 36-h period.

Physical parameterizations

The selection of appropriate physical parameterizations for global-scale modelling was performed from the following list:

Microphysics *WSM 3-class simple ice*, *WSM 6-class graupel,* *Eta*, *Thompson graupel,* *Morrison 2-moment,* *Goddard GSE;*

Longwave Radiation *RRTM;*

Shortwave Radiation *Dudhia*;

Surface Layer *ETA similarity,* *Monin-Obukhov*;

Land Surface *5-layer thermal diffusion*;

Planetary Boundary Level *Yonsei University scheme,* *Mellor-Yamada-Janjic scheme,* *ACM PBL.*

Cumulus	*Kain-Fritsch,* *Grell-Devenyi,* *Betts-Miller-Janjic.*

For the purpose of testing the listed above parameterizations have been grouped into ten different sets. All these sets have been tested for January 2001, but only the three best of them for July 2001.

2.2.3. Methods and criteria of calculation results evaluation

In order to perform evaluation of the output of the WRF model simulation results were compared with meteorological data from several sources including measurement data and GEM modelling results. Two kinds of measurements were used in the evaluation: surface measurements and upper-air observations.

To compare the precipitation fields calculated by the WRF model with measurements surface observations of daily precipitation amount from the GCOS Surface Network (GSN) were employed (www.gosic.org/gcos/GSN-data-access.htm).

Upper-air observations from the Radiosonde Database (RAOB - http://raob.fsl.noaa.gov) with 12-hour resolution were used for the comparison of computed and observed data on pressure levels. The following meteorological variables have been selected for the comparison on pressure levels: air temperature, air humidity, geopotential height, and wind speed components U and V.

To characterize the level of agreement between the calculated and measured values of meteorological variables the following statistical indicators were used: BIAS, root mean square error (RMSE), and correlation coefficient (R_{corr}). Two main types of statistics were calculated:

- spatial indicators averaged on time moments ($RMSE_{space}$, $R_{corr\text{-}space}$);
- temporal indicators averaged on sites ($RMSE_{time}$, $R_{corr\text{-}time}$).

2.2.4. Modelling results

Detailed analysis of global-scale WRF modelling results will be done on completion of the cycle of yearly calculations planned to be carried out in the near future. In this subsection only preliminary results on the basis of monthly model runs are discussed in brief. The information on air temperature and precipitation is presented in more detail than for the other meteorological variables.

The results given below are related to WRF runs with the following set of parameterizations showed the best statistics:

Microphysics	*Morrison 2-moment,*
Longwave Radiation	*RRTM;*
Shortwave Radiation	*Dudhia*;
Surface Layer	*ETA similarity;*
Land Surface	*5-layer thermal diffusion*;
Planetary Boundary Level	*Mellor-Yamada-Janjic scheme;*
Cumulus	*Betts-Miller-Janjic.*

GEM model data involved in the comparison have been obtained on the same grid using the same input information and calculation cycle (see the description above) as corresponding WRF data. The description of the set of GEM parameterizations used in global-scale modelling in MSC-E can be found in [*Tarrasón and Gusev*, 2008].

Air temperature

Global scale distributions of air temperature based on the modelling results of WRF and GEM for January of 2001 are shown in Fig.1. It can be seen that the patterns are similar. WRF temperatures over the Arctic and Antarctic regions tend to be higher that of GEM.

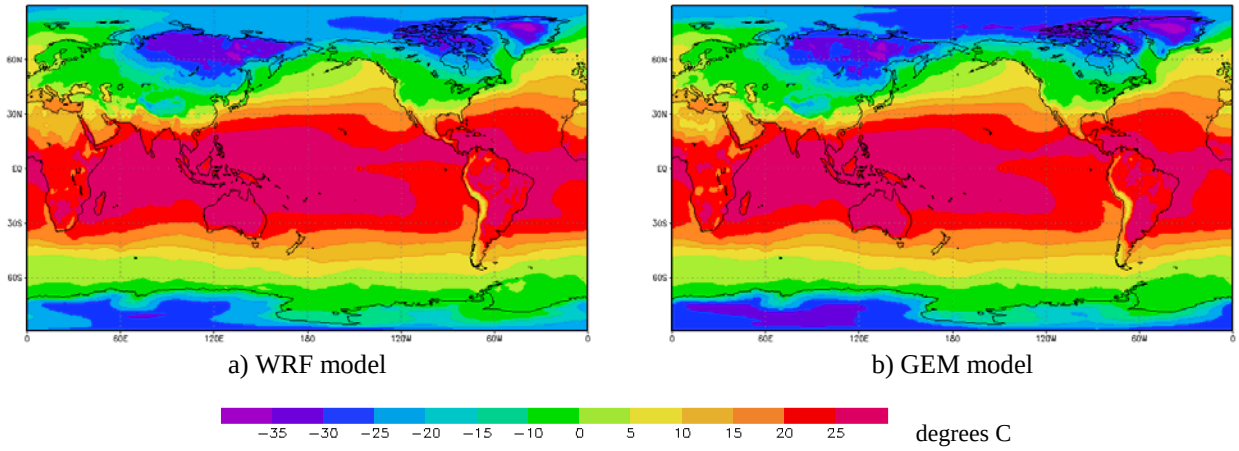

Fig. 1. *Spatial distribution of monthly mean air temperature at 2 m for January 2001 calculated by WRF (a) and GEM (b) models.*

In Table 3 results of the comparison of WRF and GEM calculations with the measurements of near-surface air temperature at the RAOB sites for January and July 2001 are presented. The better values of the statistical indicators are marked in bold. As it is seen, WRF modelling results are closer to RAOB measurements than GEM calculations for January as well as for July.

Table 3. *BIAS, RMSE, and R_{corr} statistics calculated on the basis of WRF and GEM modelling results and measurements of near-surface air temperature obtained at RAOB sites for January and July 2001.*

Model	BIAS, degrees C		$RMSE_{time}$, degrees C		$RMSE_{space}$, degrees C		$R_{corr\text{-}time}$		$R_{corr\text{-}space}$	
	Jan	Jul	Jan	Jul	Jan	Jul	Jan	Jul	Jan	Jul
GEM	**0.04**	-1.02	3.56	3.24	4.15	3.76	0.73	0.65	0.97	0.92
WRF	0.09	**-0.66**	**3.05**	**2.49**	**3.61**	**3.03**	**0.82**	**0.80**	**0.98**	**0.95**

Results of the comparison of calculated air temperature profiles for January of 2001 with measurements at the RAOB sites are given in Fig. 2. The figure contain the averaged vertical distribution of temperature measured at the RAOB sites and calculated by the WRF and the GEM models and the vertical distributions of statistical parameters RMSE and R_{corr} based on calculations and measurements.

It can be seen that time averaged calculated and measured values of temperature are close to each other, the deviations for most of the pressure levels do not exceed 1°C. The profiles of RMSE and R_{corr}

obtained on the basis of WRF model results look more preferable than corresponding profiles related to the GEM model. The difference between models is most evident for $R_{corr\text{-}time}$ profiles. This difference can be explained by the application of data assimilation in the WRF model; such an opportunity is not available in the last export GEM version.

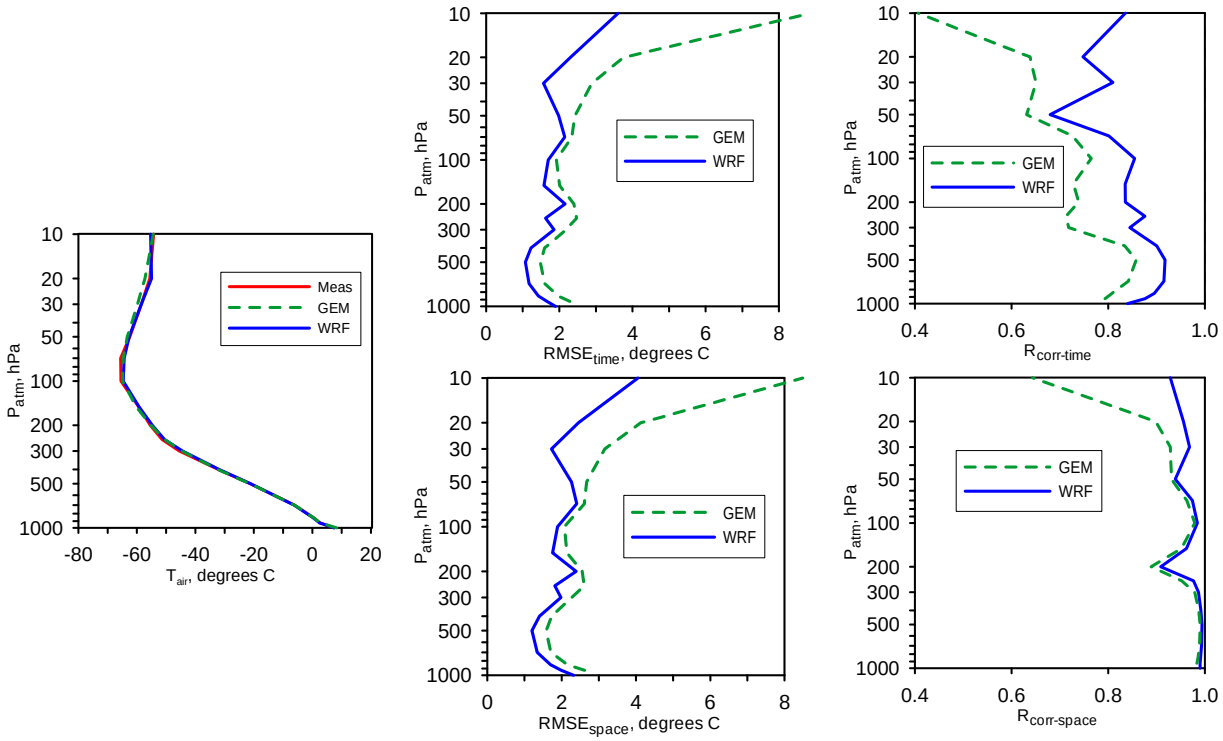

Fig. 2. *Comparison of air temperature for January 2001 obtained by WRF and GEM simulations with measurements from RAOB database.*

Along with the comparison of monthly averaged modelling results and measurement data an evaluation of model output with detailed temporal variations against the observations at individual monitoring sites was performed. In Fig. 3 the comparison of calculated and measured near-surface air temperature with 12 hour resolution is presented by the example of 3 monitoring sites chosen: 2836 in Finland, 68816 in South Africa and 72520 in the USA.

Computed variations of surface temperature for both models are in good agreement with measured values. Both models have reproduced diurnal variations for January and July of 2001 well. The correlation of computed and observed values for the WRF model is larger than for the GEM model for all the selected stations.

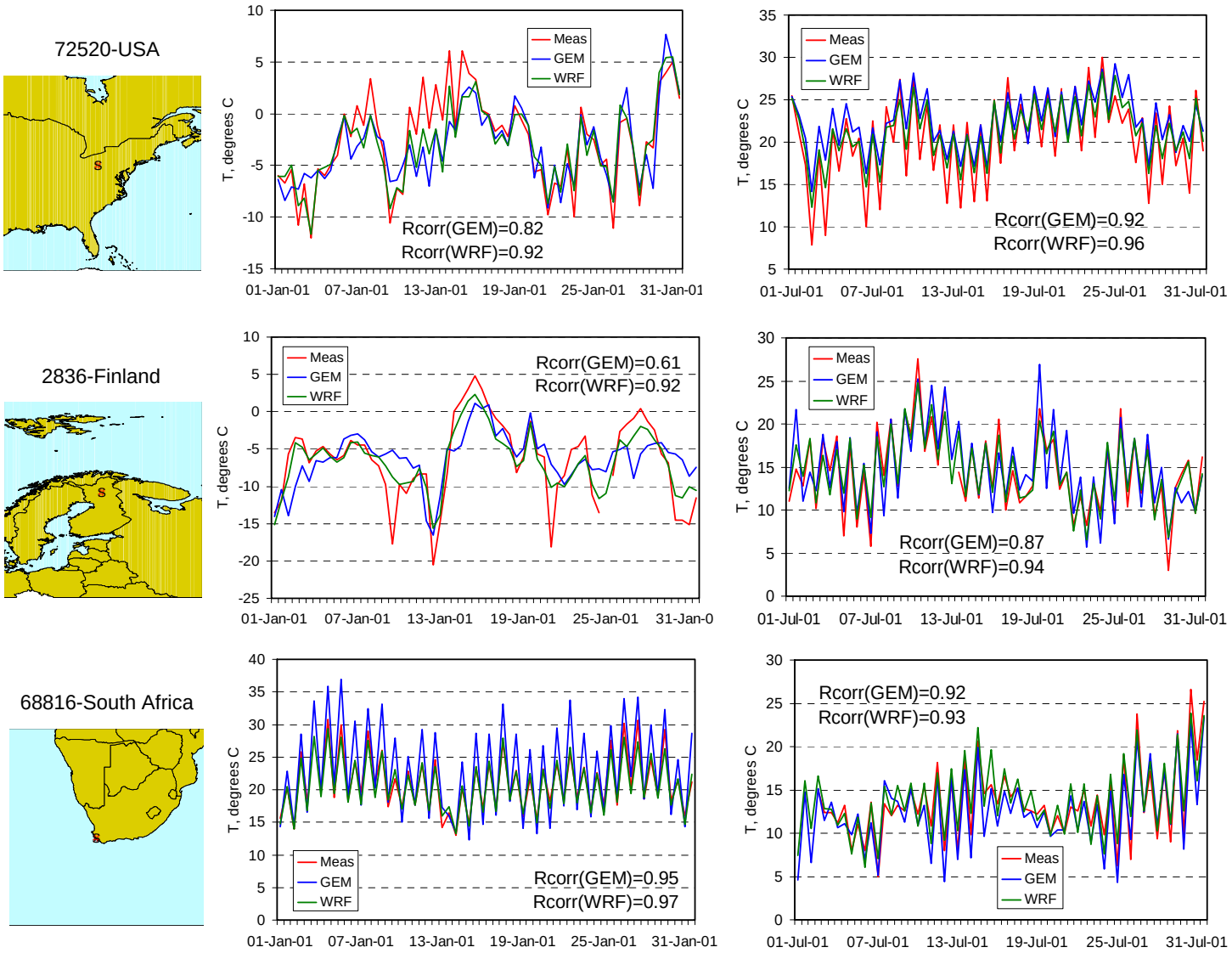

Fig. 3. *Comparison of near-surface air temperature calculated by WRF and GEM models with measurements of the meteorological sites 72520 (USA), 2836 (Finland), and 68816 (South Africa) for January and July 2001*

Air humidity, wind speed and geopotential height

Monthly mean levels, spatial distributions and temporal variations of air humidity, wind speed and geopotential height calculated by WRF are in good agreement with RAOB measurement data. The statistical indicators of agreement between WRF calculations of all mentioned meteorological parameters and RAOB measurements (RMSE and R_{corr}) look better than ones related to the GEM model both for January and for July.

Precipitation

Spatial distributions of monthly precipitation amount calculated by the WRF model were compared to the ones calculated by GEM (Fig. 4).

It can be seen that spatial patterns are similar in general. However, the precipitation amount at middle and high latitudes calculated by WRF is noticeably higher than that for GEM. The most drastic differences in the Northern Hemisphere take place in January (Fig. 4), in the Southern Hemisphere – in July (not presented here).

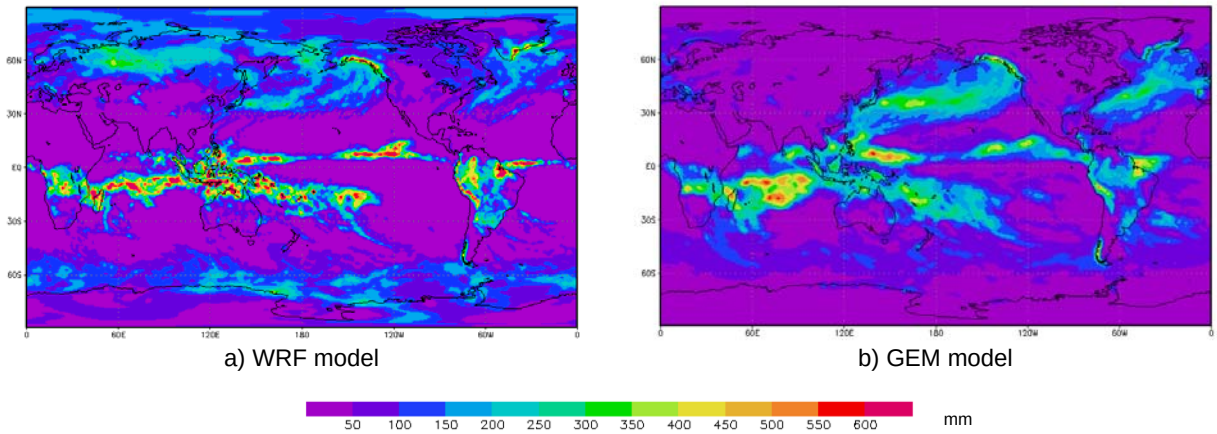

***Fig. 4**. Spatial distribution of precipitation amount for January 2001 calculated by WRF and GEM models.*

The comparison of monthly precipitation amount calculated by the WRF model versus the measurements of the GSN network for January and July 2001 has shown obvious overestimation (~27% for January and ~11% for July on average) of measured precipitation amount by WRF modelling results (Table .4). The spatial correlation of observed and calculated precipitation is not high (0.56 for January and 0.59 for July). The corresponding results for the GEM model look noticeably better.

It is significant that considerable overestimation of precipitation amount for the cold period of a year at high latitudes has been obtained for all the parameterizations listed in the first part of this subsection. To make clear the situation with precipitation in WRF additional test calculations are needed.

***Table 4.** Monthly precipitation site averages and correlation coefficients calculated on the basis of WRF and GEM modelling results and measurements of precipitation obtained at GSN sites for January and July 2001.*

Month	Monthly precipitation amount (site average)			R_{corr}	
	Measured	Calculated by WRF	Calculated by GEM	WRF	GEM
January	73	93	66	0.56	0.73
July	81	91	82	0.59	0.71

3. IMPROVEMENTS OF EMISSIONS DATA

This Chapter contains an overview of recent improvements achieved within the scientific community in the field of anthropogenic emissions inventories on a global scale.

3.1. Improvements of SO_x and NO_x global emissions data

As part of a project for the Norwegian Ministry of Environment the global version of the EMEP model has been run looking at the effects of international shipping. We had hoped to use the new EDGAR v4.0 (http://edgar.jrc.ec.europa.eu/overview.php) emission for non greenhouse gasses but this is not yet available. Until this dataset is ready a preliminary set of emissions had to be constructed.

Within the EMEP domain EMEP emissions are used. Over East Asia emissions from the ACCESS database http://www.cgrer.uiowa.edu/ACESS/acess_index.htm are used. These emissions are representative for year 2006. On the web site scaling factors for other years are given. These emissions replace an older set of emissions from *D.Streets et al.* [2003] used in previous model runs [*Jonson et al*., 2007]. Accounting for annual trends as described on the ACCESS web pages the difference in total emission levels is not large between the two datasets, but the spatial distributions are markedly different. This is mainly cased by less traffic emissions, but mare as point sources. Emissions of NH3 are not included in these datasets. Instead data from the OsloCTM2 (see below) are used for NH3. Outside the EMEP domain, emissions from international shipping are from the QUANTIFY project, described in the web pages: http://www.pa.op.dlr.de/quantify/emissions/. For scaling between different years we have assumed an annual increase in international shipping of 2.5%. For the remaining areas emissions have been adapted from the OsloCTM2 model. . These emissions are based on the EDGAR 3 data (http://www.mnp.nl/edgar/model/) and are valid for year 2000. For USA and Canada the emissions are scaled to other years based on the national totals reported to EMEP. These national totals are available through the web site: http://www.ceip.at/.

Emissions of SO_2 and NO_2 agregated as described above for year 2006 are shown in Figures 5 and 6 respectively. For SO_2 the largest sources are seen to be located in North America, Europe and in particular East Asia, For NO_2 there are also large sources over other continents. For both SO_2 and NO_2 the major shipping routes are clearly visible.

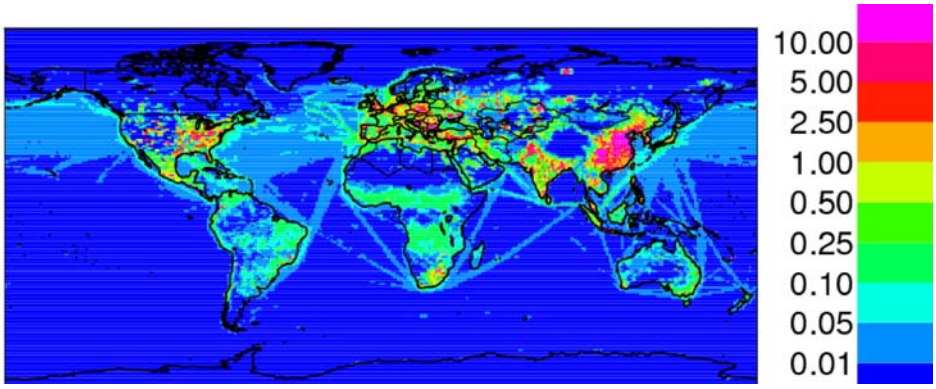

Fig. 5. *SOx emissions in g(S)m^{-2}*

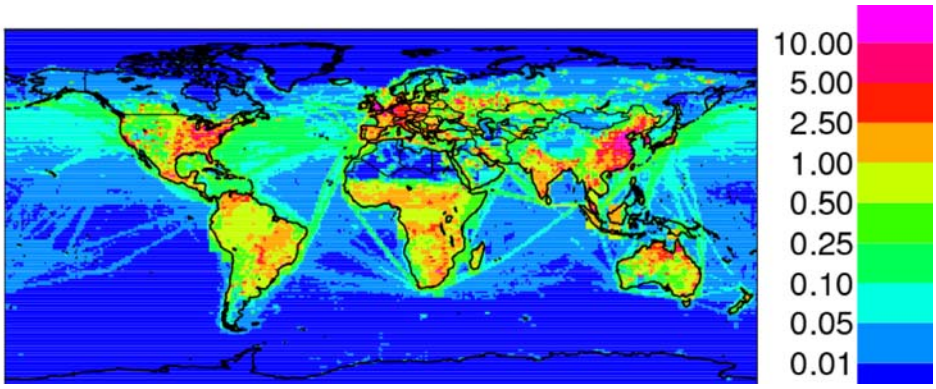

Fig. 6. *Emissions in g(N)m^{-2}*

The global model has been run for year 2006 looking at the effects of emissions from international shipping on sulphur, nitrogen and ozone formation. As an example of a comparison of model results with measurements, Figure 7 shows the tropospheric column of NO_2 in January 2006 focusing on the Mediterranean as measured by the SCIAMACHY instrument onbord the envisat satellite, and the model calculated column. The SCIAMACHY data have been interpolated to a 1x1 degree grid for easy comparison with model data

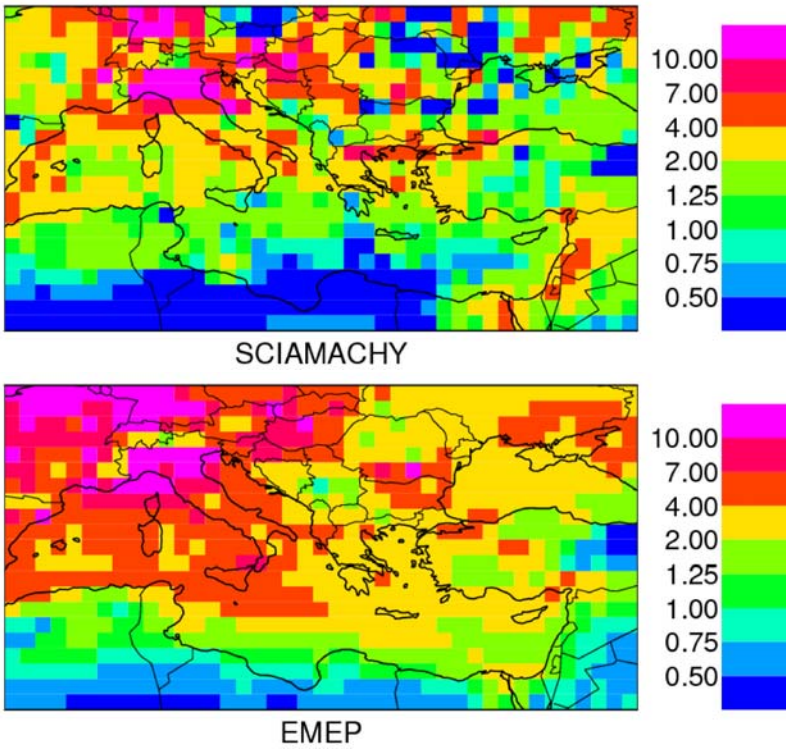

Fig. 7. *Tropospheric NO2 columns (1015 molcules cm-2) for January 2006 of NO2 measured by the SCIAMACHY satellite (top) and calculated by the EMEP global model focusing on the Mediterranean.*

Calculated NO_2 columns are in general higher than measured. However, the uncertainty in the satellite measurements is large, of the order of 35 to 60% [*Boersma et al.,* 2004]. Major source regions, as the polluted regions north and south of the Alps are seen in both measured and calculated NO_2.

3.2. Global Hg emissions inventory for 2005 and scenarios for 2020

3.2.1. Global inventory for 2005

A new global inventory of mercury anthropogenic emissions to the atmosphere was developed for 2005 within the framework of a joint AMAP and UNEP project [*AMAP/UNEP*, 2008]. The dataset has spatial resolution 0.5º×0.5º and includes three emission height levels (below 50 m, 50-150 m, above 150 m) and three types of mercury species (gaseous elemental mercury, divalent mercury compounds and particulate associated mercury). Figure 8 presents the global distribution of anthropogenic emissions of mercury in 2005.

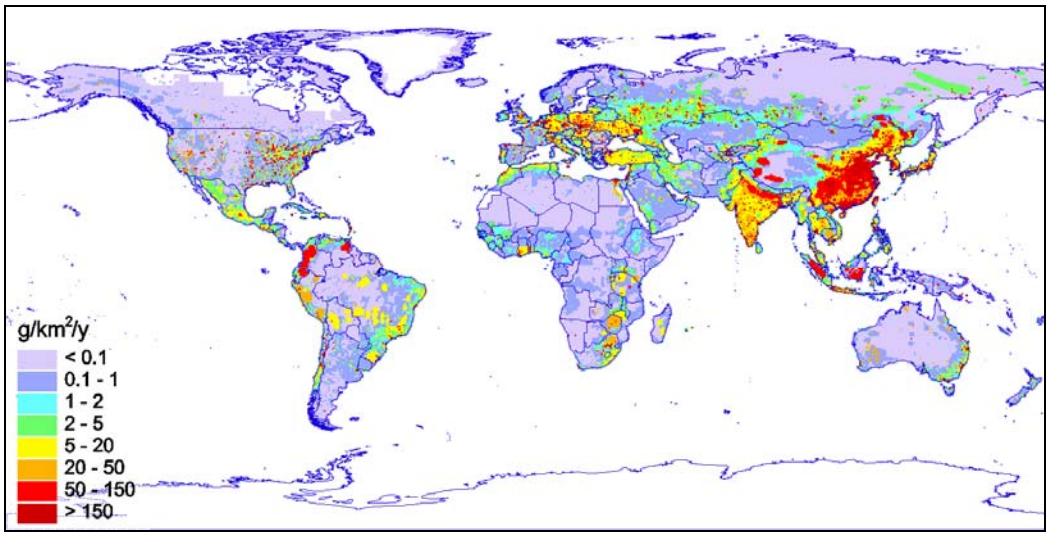

Fig. 8. *Global distribution of anthropogenic emissions of mercury in 2005, g/km²/y*

The global mercury inventory comprises of atmospheric emissions from by-product sectors, product use, cremation and artisanal mining and amounts to 1930 tonnes in total. The largest emissions of mercury to the global atmosphere from the by-product sectors occur from combustion of fossil fuels (mainly coal) in power plants, industrial and residential boilers (880 tonnes), metal production (200 tonnes) and cement production (190 tonnes). Figure 9 summarizes contribution of various anthropogenic activities to the global mercury emission.

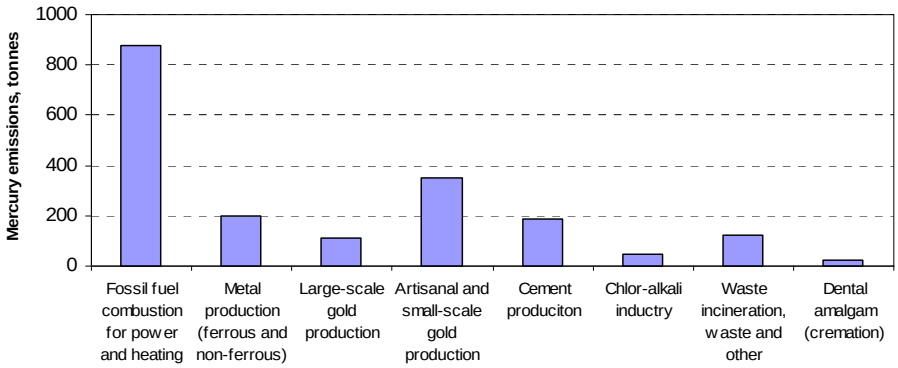

Fig.9. *Global anthropogenic emissions of mercury to air in 2005 from various sectors*

Contribution of different continents and regions to mercury emission on a global scale is shown in Fig. 10. As seen Asian emission sources contribute about 67% to the global mercury emissions whereas the contribution of European and North American sources does not exceeded 20% in sum.

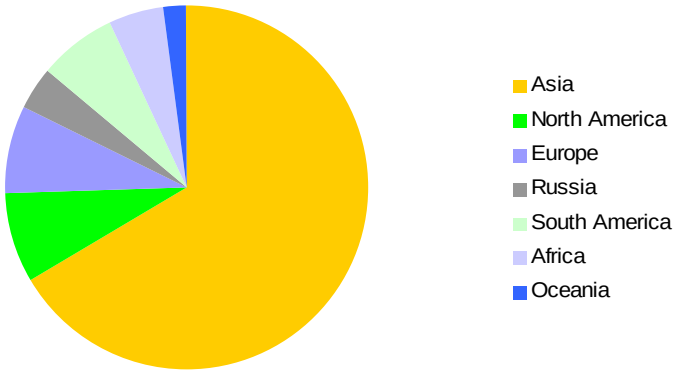

Fig. 10. *Contribution of different continents and regions to the global anthropogenic emissions of mercury in 2005*

Combustion of fuels for production of electricity and heat is the largest source of anthropogenic mercury emission in Europe, North America, Asia and Russia, and is responsible for about 40-50% of the anthropogenic emissions in Oceania and Africa. However, in South America, the artisanal and small-scale gold mining (ASGM) is responsible for the largest part of the continent emission (>55%). The ASGM emissions in some Asian countries as well as in several countries in South America account for the fact that such countries as Indonesia, Brazil and Colombia appear in the top ten ranked mercury emitting countries. China, with its more than 2000 coal-fired power plants, is the largest single emitter of mercury worldwide. Together, three countries, China, the United States and India, are responsible for about 60% of the global mercury emission in 2005 (1115 out of 1930 tonnes).

3.2.2. Emission scenarios for 2020

Future mercury emissions are dependent on a number of variables: the development of national and regional economies, development and implementation of technologies for reducing mercury emissions, possible regulatory changes, and also factors connected to global climate change.

Three emissions scenarios were considered:

- The “Status Quo” (SQ) scenario assumes that current patterns, practices and uses that result in mercury emissions to air will continue. Economic activity is assumed to increase, including in those sectors that procedure mercury emissions, but emission control practices remain unchanged.

- The “Extended Emission Control” (EXEC) scenario assumes economic progress at a rate dependent on the future development of industrial technologies and emission control technologies.

- The “Maximum Feasible Technological Reduction” (MFTR) scenario assumes implementation of all available solutions/measures, leading to the maximum degree of reduction of mercury emissions and its discharges to any environment.

Emissions scenarios for by-product sources and intentional use sectors are considered separately. A provisional first attempt to estimate global emissions of mercury from product use, cremation and artisanal gold mining was made. For emissions related to product use of mercury, the waste sector is responsible for the major part of the emissions, and better waste management, recycling and controlled incineration or landfill disposal can reduce mercury emissions substantially. For artisanal gold mining the use of mercury is likely to continue or increase since it is driven by poverty. ASGM emissions reductions are only likely to occur if emission control efforts or associated activities to provide alternative means of income result in tangible benefits to those engaged in these activities. It should be noted that the scenarios for emissions from intentional use are hypothetical and the future trends in mercury consumption are highly dependent on the development of legislation or voluntary agreements to reduce mercury usage.

Estimates of the by-product and intentional use emission sectors of mercury are shown in Figure 11 for 2005 and the three scenarios for 2020 (SQ, EXEC and MFTR). The decrease by about 40% in emissions of mercury from the by-product sector can be expected in 2020 (852 tonnes) with respect to 2005 (1483 tonnes) if the assumptions of the EXEC scenario are met. As much as 55% of the 2005 by-product can be reduced by 2020 (666 tonnes) if the assumptions of the MFTR scenario are met. These decreases in total emissions of mercury between 2005 and 2020 are clearly driven by the decreases in mercury emissions in this period calculated for the consumption of coal to produce electricity and heat.

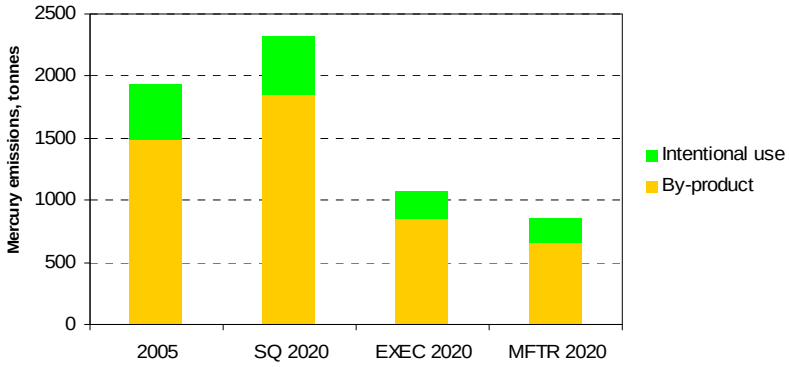

Fig. 11. *Global emissions of mercury in 2005 in comparison with three emission scenarios for 2020 (SQ, EXEC and MFTR)*

Under the EXEC scenario, clear decreases in mercury emissions between 2005 and 2020 are projected for all continents. As might be expected, the largest emissions of mercury in 2020 are estimated for Asia. The projected decreased in mercury emissions in Europe, North America, Australia and Russia are expected to be between 40 and 60%.

4. NEW MODEL DEVELOPMENTS

In this Chapter new developments performed by MSC-W and MSC-E in the field of the global scale modelling are discussed.

4.1. Acidifying pollutants, ozone and PM

Local, regional and global versions of the EMEP Unified model are all part of the same modelling system. Thus any updates in the modelling system are also implemented In the global version. Since last year there are no changes in the EMEP Unified model affecting the model results. Changes reported below are related to applications of the model or to changes in model input data.

4.1.1. Evaluation of the EMEP Unified global model in Asia

The model has been evaluated with measurements from Asia for year 2001. The evaluation has been made both with the updated Asian emissions from the ACCESS database and the older set of Asian emissions based on *D.Streets et al*. [2003]. The new set of emissions, and differences from the old set of emissions, are described in Section 3.1. For 2001 measurements of SO_2, NO_2 and O_3 are available from EANET (Acid Deposition Monitoring Network in East Asia, http://www.eanet.cc/). The sites selected for model evaluation are a mixture of urban, rural and remote sites. In the Tables 5-7 measured and model calculated annual means of SO_2, NO_2 and O_3 are listed along with correlations for the daily results. As can be expected the least satisfactory model performance is seen for the urban and partially also for the rural sites. These sites are all close to major sources that can not be resolved by the coarse 1 x 1 degrees) resolution in the model. As a result SO_2 and NO_2 levels are underpredicted by the model at virtually all the urban and rural sites, and correlations are in general poorer for all three species compared to remote sites. With the updated set of emissions correlations are in general slightly but consistently higher. As the total emission levels is virtually the same in the two emission sets for Asia, this is a clear indication that the distributions between sectors, and the resulting spatial distributions of the emissions, represent an improvement.

Table 5. *Observations of SO2 ($\mu gS\ m^{-3}$) from EANET compared to model calculations with original and updated ACESS emissions. Corr. is correlations.*

	Site	Observation	Original run	Corr.	ACESS run	Corr.
Urban	6: Hongwen (China)	6.61	0.99	0.10	1.22	0.15
	8: Xiang-Zhou (China)	10.87	2.47	0.19	2.83	0.20
	23: Banryu (Japan)	233	0.82	0.06	0.88	0.07
	37: Bangkok (Thailand)	14.70	1.10	0.25	1.30	0.29
	38: Samutprakarn (Thailand)	11.49	1.12	0.39	1.31	0.43
Rural	2: Jinyunshan (China)	1.60	2.00	0.15	1.11	0.14
	4: Weishuiyuan (China)	2.69	2.51	-0.07	4.16	-0.07
	23: Ijira (Japan)	1.81	2.48	0.42	1.15	0.40
Remote	14: Rishiri (Japan)	0.40	0.09	-0.06	0.09	0.00
	15: Tappi (Japan)	0.67	0.18	0.18	0.15	0.20
	17: Sado (Japan)	0.63	0.21	0.23	0.17	0.22
	18: Happo (Japan)	0.86	1.77	0.34	0.96	0.31
	19: Old (Japan)	0.77	0.45	0.10	0.41	0.08
	20: Yusuhaia (Japan)	0.93	1.70	0.12	1.53	0.27
	21: Hedo (Japan)	0.44	0.52	0.04	0.35	0.08

Table 6. *Observations of NO_2 ($\mu gN\ m^{-3}$) from EANET compared to model calculations with original and updated ACESS emissions. Corr. is correlations.*

	Site	Observation	Original run	Corr.	ACESS run	Corr.
Urban	6: Hongwen (China)	11.38	0.96	0.20	0.84	0.27
	8: Xiang-Zhou (China)	13.30	2.06	0.30	1.27	0.30
	23: Banryu (Japan)	1.33	0.55	0.05	0.49	0.07
	37: Bangkok (Thailand)	3.84	0.84	0.06	0.65	0.18
	38: Samutprakarn (Thailand)	6.24	0.88	-0.22	0.66	-0.28
Rural	2: Jinyunshan (China)	13.24	6.73	0.20	4.91	0.25
	4: Weishuiyuan (China)	6.80	9.90	0.02	3.36	0.08
	23: Ijira (Japan)	1.22	0.62	0.16	0.23	0.08
Remote	14: Rishiri (Japan)	0.26	0.06	0.23	0.07	0.25
	15: Tappi (Japan)	0.58	0.11	0.26	0.09	0.26
	17: Sado (Japan)	0.83	0.13	0.32	0.10	0.20
	18: Happo (Japan)	0.97	0.58	0.04	0.25	0.02
	19: Old (Japan)	0.84	0.30	0.17	0.26	0.18
	20: Yusuhaia (Japan)	1.50	0.95	0.02	0.74	0.06
	21: Hedo (Japan)	0.40	0.29	0.04	0.11	0.17

Table 7. *Observations of O_3 (ppbv) from EANET compared to model calculations with original and updated ACESS emissions. Corr. is correlations*.

	Site	Observation	Original run	Corr.	ACESS run	Corr.
Urban	23: Banryu (Japan)	36.11	42.70	0.30	41.99	0.30
	38: Samutprakarn (Thailand)	4.52	21.80	0.10	22.92	0.13
Rural	23: Ijira (Japan)	29.65	32.51	0.13	31.71	0.17
Remote	14: Rishiri (Japan)	38.13	33.10	0.56	32.49	0.58
	15: Tappi (Japan)	46.56	37.61	0.64	36.80	0.67
	17: Sado (Japan)	41.02	43.64	0.52	42.73	0.56
	18: Happo (Japan)	53.29	35.96	0.25	34.8	0.31
	19: Old (Japan)	44.62	45.14	0.52	44.64	0.49
	20: Yusuhaia (Japan)	28.91	33.76	0.29	32.63	0.30
	21: Hedo (Japan)	42.89	34.53	0.67	33.92	0.68

Compared to model evaluations comparing with measurements in Europe [i.e. *Jonson et al.*, 2007], the agreements between model and measurements leaves much to be desired. This is most likely caused by a poorer quality in model input data such as emissions and landuse data. In the MISC II study [*Carmichael et al.*, 2008] results from several regional models have been compared to measurements from EANET. The horizontal model resolution in the regional models are a factor of two or higher. Despite the higher resolution in the regional models, the model performance of the EMEP model is in the same range as the ensemble of the MICS models for the species analyzed (SO_2, NO_2, O_3).

4.1.2. On-going model development: Convective washout in EMEP Global model

Convection is an effective process for vertical exchange of heat, momentum and mass. In the atmosphere it is most often caused by solar heating of the surface, especially in low latitudes. The chain of processes can be briefly summarized as follows: near surface air is heated by sunlight as a result the air density decreases resulting in convective instability and upward motion of air and vertical

mixing of tracers. The vertical flow is generally further enhanced by the release of heat when humidity in the rising air condenses.

The importance of convection in atmospheric chemistry, air pollution and climate is caused by the fact that convective processes can transport near-surface pollutants more rapidly into the free troposphere than large scale motion. A well-known example are ozone precursors such as NO_x and hydrocarbons, which have major emission sources at the surface and exhibit a non-linear behaviour in terms of ozone-production efficiency. Transported into the free troposphere, NO_x has a larger ozone yield per molecule than at the surface where concentrations are higher. The upper troposphere is limited in hydrocarbons, so that transport from the surface has the overall effect of increasing ozone at the top of convective cells.

In addition, vertical transport of air often leads to convective rainfall by which water-soluble gases and particles are washed out (wet deposition) and efficiently transported through the atmospheric column, and in many cases removed completely by rain reaching the surface.

However, vertical transport is important not only for the height distribution of concentrations and chemical production/destruction efficiencies, but also for long range transport. Large-scale flow occurs primarily in the free troposphere. Convective events efficiently move pollutants from the boundary layer into the free troposphere where they can be readily transported over large distances, dependent on their chemical life-times and water solubilities.

In air pollution and climate models, convection is usually grid-resolved in the vertical, but subgrid in the horizontal dimensions. This fact, combined with the importance of convection for distribution of gases and particles, calls for parameterization that relate convective transport and washout to other fields that are grid resolved.

Implementation in EMEP Model

In order to implement convection in a chemical transport model, we need to distinguish three processes: a) the process of convection as predicted by a meteorological model, b) the vertical transport of humidity, gases and particles in grid columns with convective activity based on fields of motion from the underlying meteorological model, and c) the uptake of water-soluble gases or particles, often followed by rain-out. EMEP model will be using the same parameterization used in OsloCTM2 model, which is a chemistry transport model driven with ECMWF meteorology. OsloCTM2 uses the convective mass flux scheme of *M.Tiedke* [1989] same as used at ECMWF Integrated Forecast System (IFS) model. This gives convective mass fluxes and convective rain as outputs. The convective transport of chemical species is developed by M. Prather and B. Hannegan of University of California at Irvine (UCI) using the vertical gradient of convective mass fluxes together with mixing ratios information and second-order moments. Convective washout is implemented by *T. Berntsen* (University of Oslo), described by [*Berglen et al.*, 2004], using temperature, pressure, specific humidity, large scale rain, convective rain, and convective mass flux provided by ECMWF. In addition to IFS meteorological data, EMEP will be using PARLAM-PS meteorology as input.

Different kinds of convection to be considered are:

deep convection:

- extending from the boundary layer to the upper troposphere
- connected with large-scale convergent flow

- maintained by large-scale moisture convergence
- accompanied by precipitation.

midlevel convection:

- extending from one atmospheric layer to another
- connected with potentially unstable air above the boundary layer
- maintained by large-scale moisture convergence

shallow convection:

- trade-wind cumuli are one example of this type of convection
- mostly non-precipitating, maintained by supply of moisture from surface evaporation.

As of today, convective transport is treated in the EMEP model as part of the vertical exchange routine, with effective vertical diffusion coefficients. Previously this method has been sufficient as EMEP focused on regions where vigorous convective events are rare. However, ina global model comprising equatorial regions and assessing long-range transport of pollutants also in low latitudes, a more adequate parameterization of convection is necessary.

All meteorological parameters needed, such as upward vertical mass fluxes, rain etc. have been already included also in the new PARLAM-PS data and are ready to be used in the global EMEP model version. However a discussion is still active about the advection scheme. Furthermore, all EMEP applications feature higher resolutions down to a few kilometres, where convection may be partly grid-resolved. This requires flexible coding, so that the same convection routine in the global EMEP model version can also be used in the regional and local scale applications. At high resolution, the vertical updraft can be calculated from horizontal wind convergence. To create a flexible code, convection and advection can be combined and done at the same time in one routine even in a coarse-resolution model.

As explained above, work to improve the convective parameterization in EMEP is initiated and well under progress. Convective washout is already coded in and facing some technical problems at the moment with parallelization etc. Any progress will be reported in due time.

4.2. Heavy metals and POPs

New model developments for heavy metal and POP modelling on a global scale related to further development of the GLEMOS modelling system. They include elaboration of a pilot modelling framework with modular architecture for heavy metals and persistent organic pollutants (POPs), implementation of the nesting procedure and development of the multi-media approach for mercury modelling.

4.2.1. Architecture of the multi-pollutant, multi-media modelling framework

The global modelling framework is being developed within EMEP as a flexible research tool for a wide variety of tasks under the Convention. The motivation and main requirements for the modelling framework were formulated in the previous progress report [*Tarrasón and Gusev*, 2008]. They include a flexible choice of the model domain and grid resolution, multi-pollutant and multi-media approach, a

modular model architecture and computational efficiency. Some of these requirements are already implemented in the current versions of MSC-W and MSC-E global models (such as flexibility of the model domain and grid resolution). In order to evaluate the entire concept and to facilitate the framework development MSC-E undertook efforts to elaborate a pilot version of the framework for heavy metals and POPs based on the newly developed global model GLEMOS. The aim of this study was to develop the model architecture with essential modular structure for the multi-pollutant and multi-media modelling system. The model architecture has been successfully developed and tested as a part of new version of the GLEMOS model. Main features of this architecture are discussed below.

The GLEMOS (Global EMEP Multi-media Modelling System) is an Eulerian type chemical transport model with variable spatial resolution and model domain. It is driven by off-line meteorological data provided by a meteorological pre-processor (a number of modern weather forecast models are supported – GEM, WRF). An overview of the base characteristics of the model are given in [*Tarrasón and Gusev*, 2008]. The atmospheric part of the model was evaluated in the TF HTAP model experiment (TP1x) along with other transport models. Current version of the model includes parameterizations for heavy metals and POPs but the general modular architecture implies possibility to extend the list of substances.

A modular architechture will enable the user to configure the model suitable for a particular application by selecting different sets of modules. In particular, it provides the flexibility to simulate pollutants with very different properties (e.g. ozone and POPs) either all together (similar to the “one atmosphere” approach) or separately using less computer resources. It also allows considering different number of environmental media depending on a pollutant properties: only the atmosphere for pure air pollutants or also other media (soil, vegetation, the ocean etc.) for pollutants with complex environmental cycling.

The modular architecture has been implemented in the GLEMOS model code. The general model scheme reflecting the modular structure is presented in Fig. 12. Each environmental medium is presented in the model by a set of procedures describing general processes in the medium which are combined into the program modules. Each module can be attached or detached from the model at the compilation stage using command scripts. All pollutants are combined in groups of substances with similar properties (e.g. particulate heavy metals, POPs etc.). Each pollutant group is presented in the model by a number of modules defining the pollutant properties and behaviour in each environmental media. Besides, each pollutant can be characterized by different physical forms or chemical compounds specific for each media. The pollutant groups can be attached to the model using the procedure similar to that for media.

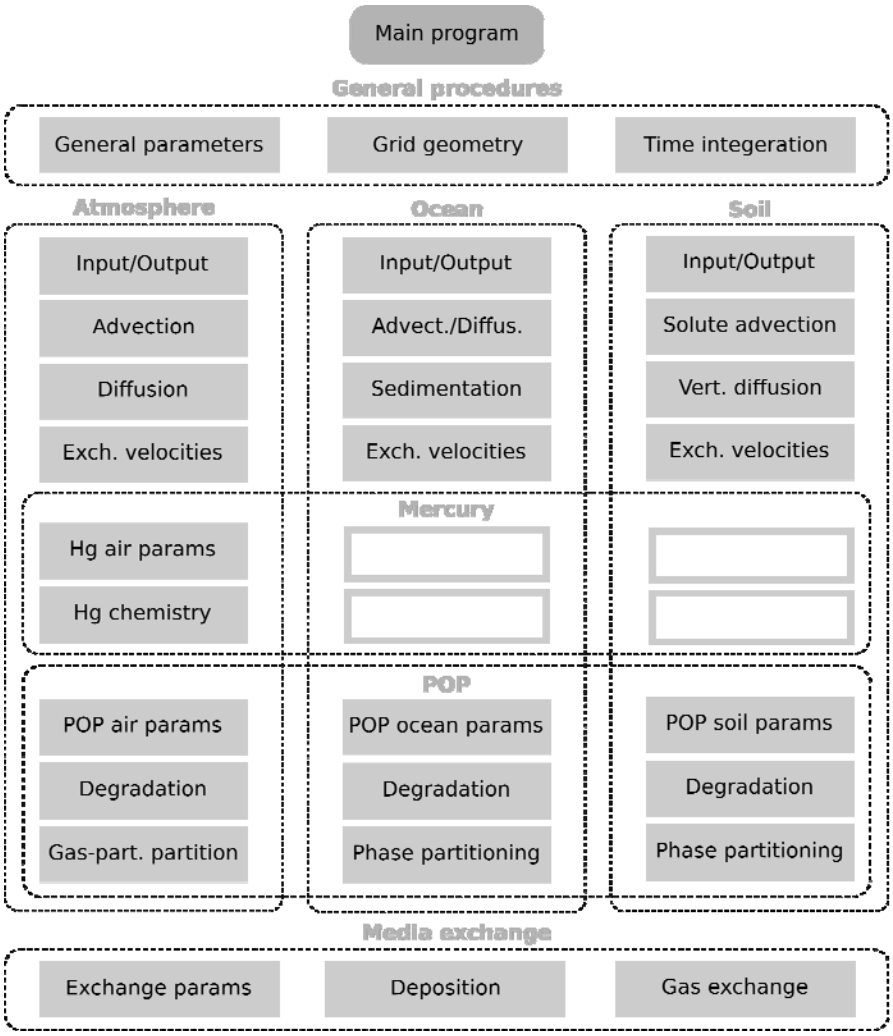

Fig. 12. *General scheme of the multi-media, multi-pollutant framework architecture*

Three pollutant groups have been included into the current version of the model: mercury, particle-bound heavy metals (Pb, Cd) and POPs (only two groups are shown in the figure for illustration purpose). Parameterizations of media processes for these pollutants applied in the model are largely based on the previous well developed and extensively tested hemispheric models MSCE-HM-Hem and MCSE-POP-Hem. Available parameterizations of mercury and particulate heavy metal groups included only the atmosphere and were adapted for appropriate atmospheric modules of GLEMOS. Pilot results with applications and evaluations of these modules are presented in Subsection 4.2.2. Besides, development of the multi-media approach for mercury modelling has been initiated and the first results are discussed in Subsection 4.2.4. On the other hand, a consistent multi-media approach has been developed for POPs previously [*Gusev et al*., 2005] and it has been adapted for appropriate media modules of GLEMOS including the atmosphere, the ocean, soil and vegetation. Extensive testing of these modules are planed for the near future.

As mentioned above the modular architecture provides a flexible means to include other pollutants to the model. Simulation of heavy metals and POPs requires input information on air concentration of some other substances including ozone, OH-radical, sulphur dioxide, PM, etc. Currently, appropriate pollutant groups are presented in the model by simplistic modules reading input information generated by third parties – GEMAQ-EC (Environment Canada), MOZART (Max Planck Institute for Meteorology, Germany). But there are also plans to supply the modelling framework with full-scale modules simulating these substances, primarily, based on the parameterizations available within EMEP and in

close co-operation with MSC-W. These modules could be used both on-line along with heavy metals and POPs simulations or in an off-line mode pre-calculating required reactants concentrations.

The multi-scale approach implemented in the modelling framework allows simulations both on a global and regional scales with variety of spatial resolutions ranging from several angular degrees down to tenths of degree (several kilometres). Appropriate model configuration is defined by command scripts including possibility to set up boundary conditions for regional modelling. To improve coupling between different scale simulations a nesting procedure is being developed. The first experiences with the nesting procedure implemented in GLEMOS are described in Subsection 4.2.3 of this report.

4.2.2. Pilot calculations of heavy metal pollution on a global scale

The developed global modelling framework described above was tested for two heavy metals with diverse properties – lead and mercury. These two substances relate to different pollutant groups according to the framework classification and, therefore, functionality of the multi-pollutant modular approach was also examined. For the testing purpose we performed annual simulation run with 1×1 degrees resolution using meteorological dataset for 2001 generated with GEM.

LEAD

The only available global dataset of lead anthropogenic emissions related to 1990 [*Tarrasón and Gusev*, 2008] was used in the study. No natural emission or wind re-suspension were considered. In this aspect, lead can be considered as a tracer-like pollutant with relatively short life time (days to weeks) in the atmosphere with respect to dry and wet removal. Therefore, annual deposition pattern presented in Fig. 13 demonstrates essentially regional character of lead pollution over long periods. There is almost no effect of the intercontinental transport on pollution levels in different regions.

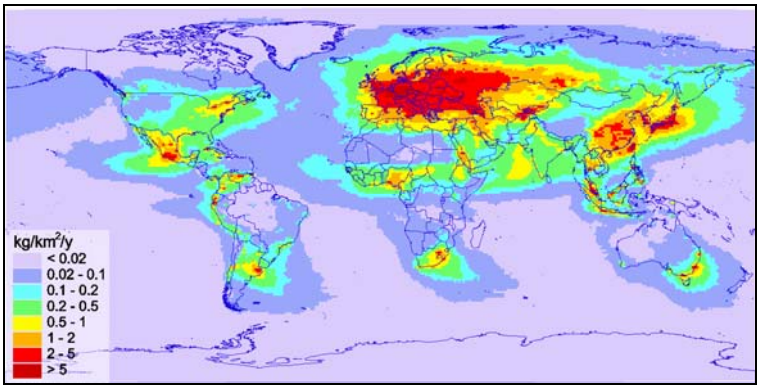

Fig. 13. *Total annual deposition of lead*

Nevertheless, episodic transport of lead can cover significant distances between the continents or can achieve remote regions. Figure 14 shows simulated episode of lead transport from sources located Central Asia, southern Ural and Siberia to the Arctic in winter (January 13-16, 2001). The plume originated in Central Asia and Southern Siberia in two days reaches northern regions of Russia, is amplified by strong source located in Northern Siberia (Norilsk) and goes further to the Arctic. During next two days it reaches the coast of Greenland.

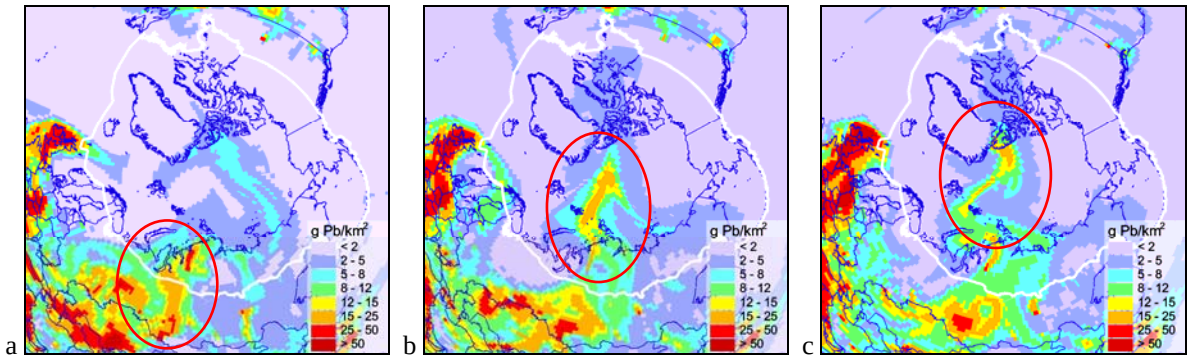

Fig. 14. *Daily mass of lead in air column showing episode of lead entrainment to the Arctic from Central Asian and Siberian sources (January 13-16, 2001): (a) – January 13; (b) – January 15; (c) – January 16*

An example of comparison of the simulation results with observations is presented in Fig. 15. It should be noted the comparison is not straightforward because of the inconsistency between the reference simulation as well as monitoring year 2001 and emissions data related to 1990 (the only available global dataset). During this 10-years period emissions of lead decreased essentially in European countries (from several times to an order of magnitude). Therefore, one can expect significant overestimation of measured values by the model at most inland European monitoring sites. However, at remote sites only partly affected by major European emission sources, at least, qualitative comparison is possible. For example, the model successfully reproduced seasonal variation of lead concentration in the Arctic measured at site Zeppelin, Spitsbergen (NO42) (Fig. 15a). Particularly, the model caught high wintertime concentrations typical for the Arctic haze and low concentrations during summer. Besides, the model reproduced variation of lead concentration in precipitation at another remote site Porspoder (FR90) located at the headland of the Atlantic coast of France jutting out into the ocean (Fig. 15b).

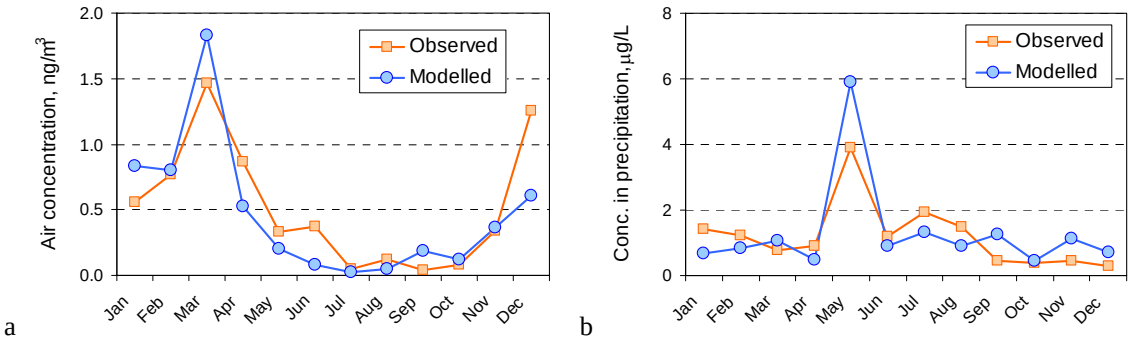

Fig. 15. *Comparison of modelled and observed lead air concentration at the Arctic site Zeppelin, Spitsbergen (NO42) and concentration in precipitation at remote site Porspoder, France (FR90) in 2001*

MERCURY

Mercury is a more complicated pollutant characterized by intensive chemical transformations in the atmosphere. The original mercury chemical scheme from the hemispheric transport model MSCE-HM-Hem was adapted for appropriate chemical module of the GLEMOS framework. A recently developed global anthropogenic emission dataset for 2005 was used in the study [*AMAP/UNEP*, 2008; Section 3.2]. Besides, we utilized natural emissions dataset based on distribution of the global estimate

[*Mason*, 2009] over the Earth's surface depending on mercury content in soils and the surface temperature for land and primary productivity of carbon for the ocean. Preliminary results of the model simulation are shown in Fig. 16. Available observations of mercury in air and wet deposition flux from the EMEP, NADP/MDN and CAMNet monitoring networks as well as from literature are presented for comparison. As seen even these first results demonstrate satisfactory agreement with measurements. Elevated concentrations of gaseous elemental mercury (GEM) are characteristics of regions with high anthropogenic and natural emissions (Fig. 16a). Besides, the ambient concentration exhibits pronounced south-to-north gradient from 1.1 to 1.8 ng/m^3. Significant wet depositions mostly take place over low and temperate latitude where major emission sources are located and most intensive precipitations take place (Fig. 16b).

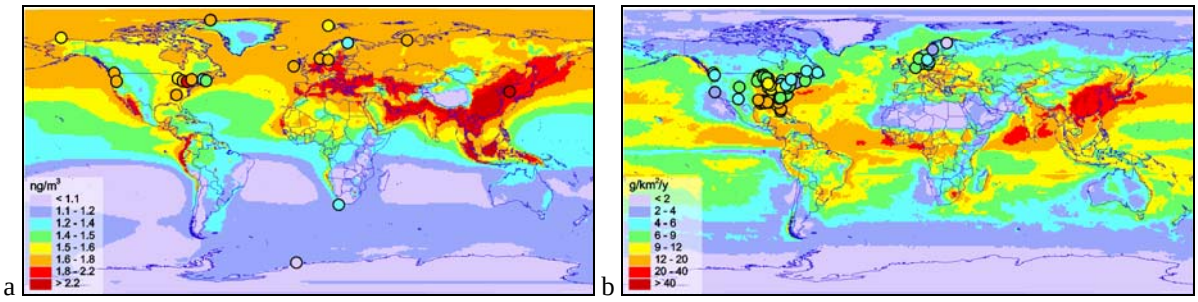

Fig. 16. *Annual mean concentration of elemental gaseous mercury in the ambient air (a) and mercury wet deposition flux (b). Circles present long-term measurements from the EMEP, NADP/MDN and CAMNet monitoring networks as well as from literature .*

More detailed comparison of modelled results with measurements is shown in Fig. 17. Simulated GEM concentrations well correlate with observations and the bias is negligible. The agreement for wet deposition flux is somewhat worse than that for concentration. The model tends to somewhat overestimate measured fluxes and correlation is lower. Nevertheless, in the most cases the model-to-measurement deviation does not exceed a factor of two.

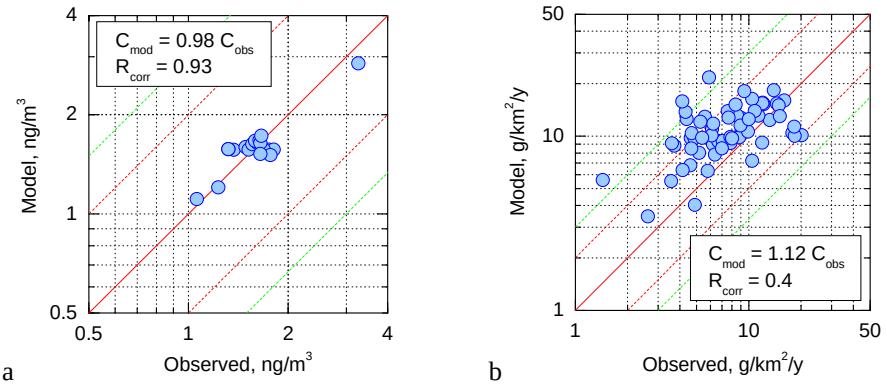

Fig. 17. *Scatter plots of model-to-measurement comparison of elemental mercury concentration (a) and wet deposition flux (b). Red solid line delineates 1:1 ratio, red and green dashed lines show deviation by a factor of two and three, respectively*

Nevertheless, more thorough evaluation of modelling results is required along with further improvement of the mercury chemical scheme in accordance with new findings of the scientific community. Besides, additional efforts to evaluate mercury natural emission and air-surface exchange are needed. First steps in this direction are discussed in Subsection 4.2.4.

4.2.3. Implementation of nesting procedure

Support of air pollution modelling at different spatial scales, from global to regional and local ones, is an important feature of the developed global modelling framework. Different approaches can be used for implementation of the multi-scale modelling. In particular, the variable resolution modelling can be applied to refine the model resolution over an area of interest, which allows to gradually condense model grid in the selected areas. Another possible approach to the multi-scale modelling is the one-way or two-way nesting of several model domains with different resolution. Selection of particular approach depends on the nesting capabilities of a meteorological driver required to generate meteorological input with necessary spatial resolution.

The work on the development of the nesting capabilities of the EMEP global modelling framework has been recently initiated with the implementation and testing of the one-way nesting approach. The one-way nesting assumes the link of coarse and fine resolution modelling through application of initial and boundary conditions with necessary spatial and temporal resolution. The modelling framework will provide flexible definition of the model domains and their spatial resolution.

Modelling experiments with the nesting were carried out for lead atmospheric transport in 2001. The model simulations were performed for two domains shown in Fig. 18 – the global model domain with spatial resolution 1°x1° and the fine resolution domain covering part of the European region with spatial resolution 0.25°x0.25°. Gridded emission datasets for the coarse and the fine resolution modelling were compiled based on the global emission inventory of lead for 1990 and the EMEP official emissions data for 2001. To investigate the effect of the refinement of spatial resolution on the model estimates of pollution levels the emissions of large point sources of lead available within EMEP and in the EPER databases were used. Necessary meteorological input for the global and regional scale modelling was prepared for the year 2001 using the global meteorological model GEM.

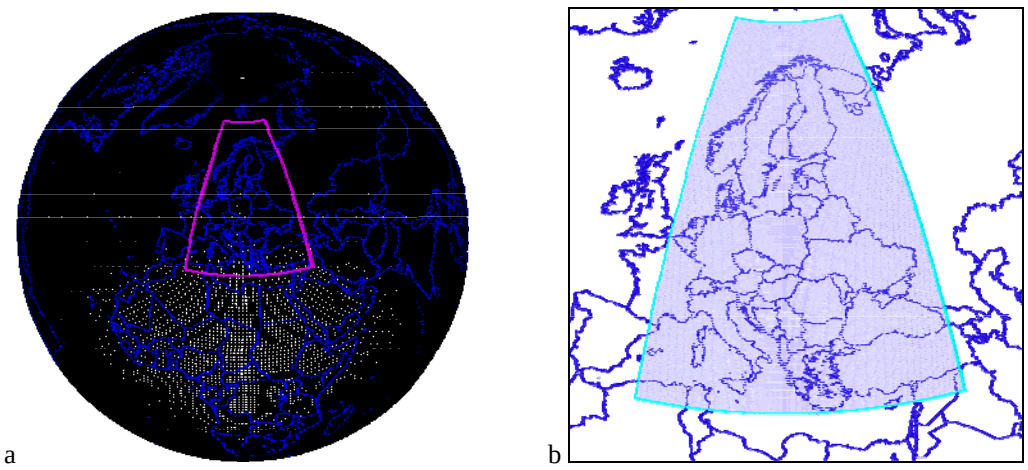

Fig. 18. *Configuration of model domains for the nesting experiments: (a) coarse model grid with resolution 1°x1° for global scale modelling, (b) fine model grid with resolution 0.25°x0.25° for modelling over Europe*

Test simulations of lead atmospheric transport on global scale were carried out for three months of 2001, namely, from January to March. The fine resolution modelling was performed for March of 2001 using generated initial and boundary conditions. Preliminary results of the one-way nesting of the fine resolution model run within the global scale model run are shown in Figs. 19 and Fig. 20. The figures present spatial distribution of monthly mean air concentration and monthly deposition of lead over the selected part of European region with coarse and fine spatial resolution. It can be seen that the

increase of spatial resolution essentially affects the distribution of lead concentration and deposition near emission sources providing more detailed description of pollution levels. Preliminary comparison of modelling results with measurements of lead concentrations for 2001 indicated better correlation of fine resolution lead concentrations in comparison with the coarse resolution results.

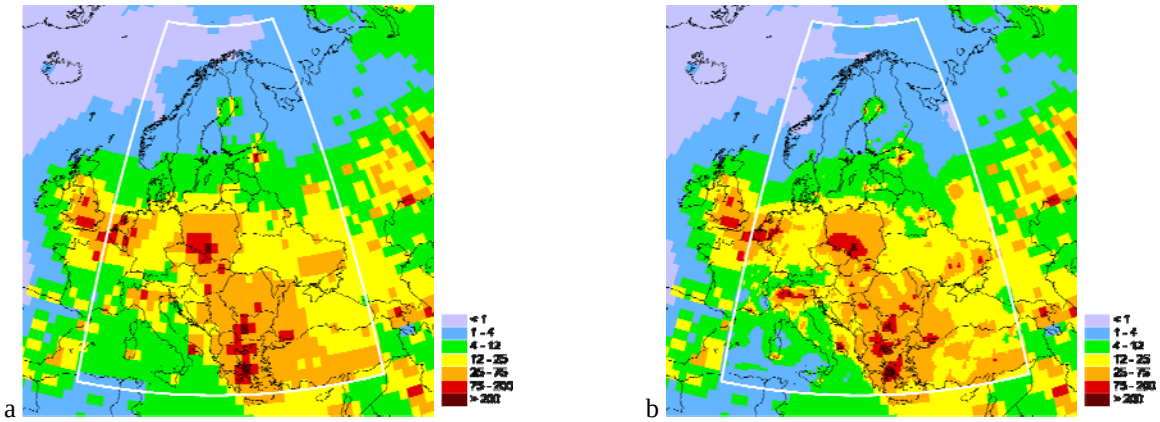

Fig. 19. *Spatial distribution of monthly mean lead air concentrations (ng/m^3) for March 2001 with coarse spatial resolution 1°x1° (a) and with refined spatial resolution 0.25°x0.25° over the selected part of European region*

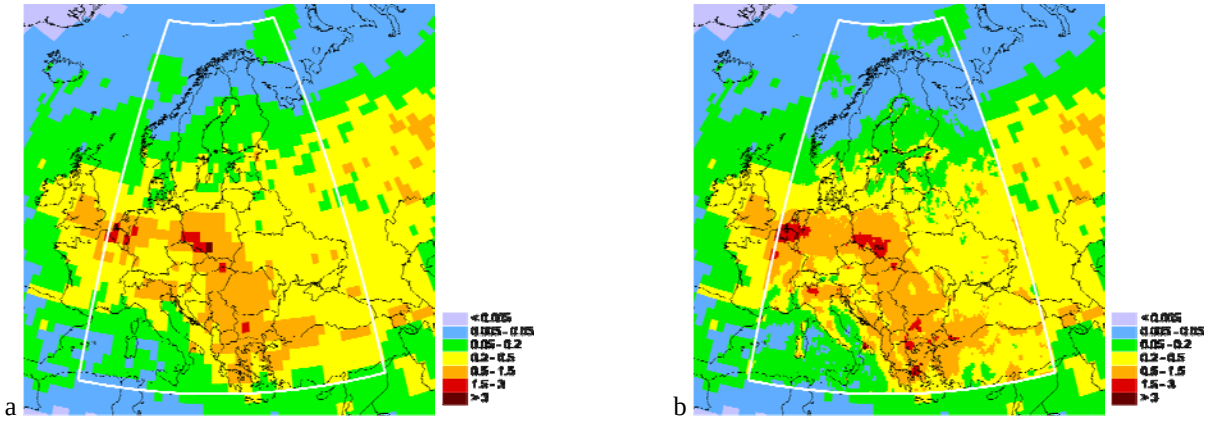

Fig. 20. *Spatial distribution of total monthly lead deposition (g/km^2/month) for March 2001 with coarse spatial resolution 1°x1° (a) and with refined spatial resolution 0.25°x0.25° over the selected part of European region*

4.2.4. Development of mercury multi-media modelling approach

Mercury as a relatively volatile pollutant is characterized by intensive cycling between different media. Once emitted to the atmosphere from anthropogenic or natural sources it is transported globally (mostly in elemental gaseous form) until it is transformed to one of hydrophilic oxidised forms and deposited to the ground. After entering into soil or seawater, oxidized mercury can be transformed to bio-available methylmercury form or reduced back to volatile elemental form with subsequent re-emission to the atmosphere. Thus, mercury dispersion in the environment has complicated character including both atmospheric transport, chemical transformations and continuous exchange with other media. This aspect should be taken into account in the assessment of mercury contamination and, in particular, long-term dynamics of mercury pollution levels – historical trends and future scenarios.

In order to take into account mentioned above peculiarities of mercury dispersion MSC-E initiated development a multi-media approach for mercury modelling. For development purpose, a simplified low-resolution version of the global modelling framework (GLEMOS-LR) was applied. Major distinctions of this version from the full-scale model include significantly lower spatial resolution – 20º×20º (Fig. 21a), simplified atmospheric and oceanic dispersion schemes and use of averaged meteorological and oceanic driving fields presenting 'climatic' conditions. All these aspects make the GLEMOS-LR model to be a very useful tool for development and testing new parameterisations and for application to very long-term simulations (scale of centuries) for evaluation of the pollutant accumulation and cycling in the environment.

The model includes three environmental media – atmosphere, ocean and soil – with appropriate exchange fluxes (Fig. 21b). Model description of the processes governing mercury fate cycling in different media is presented below in more details.

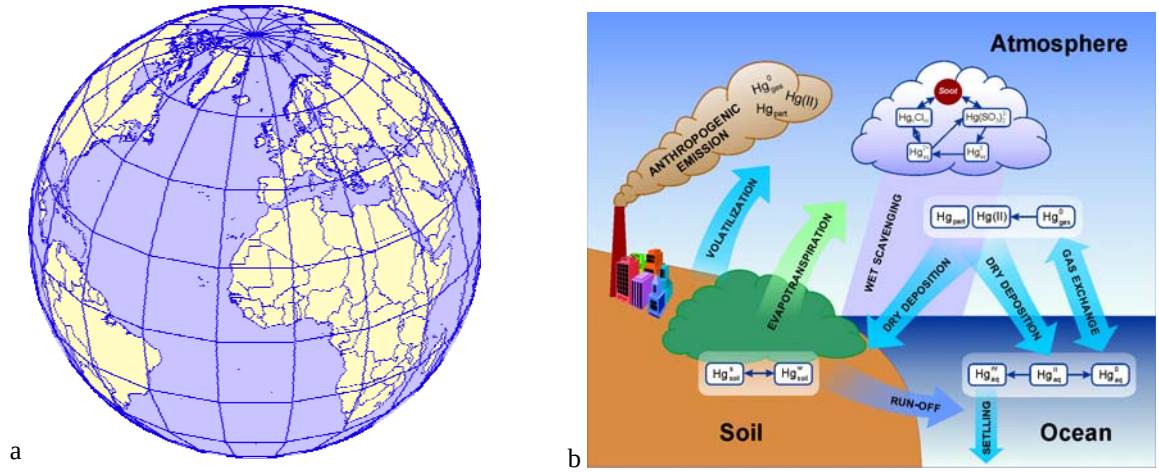

Fig. 21. *Horizontal structure of the model domain (a) and general scheme of media and exchange processes considered in the model (b)*

Atmosphere

The atmospheric model domain consists of 13 irregular model layers and covers global atmosphere up to 30 km altitude (Fig. 22). Atmospheric dispersion and other processes are driven by meteorological fields based on the ECMWF ERA-40 re-analysis (http://data-portal.ecmwf.int/data/d/era40_daily/) averaged over a long period in order to obtain 'climatic' conditions. In particular, the original data with 2.5º×2.5º spatial and 6-hours temporal resolution were aggregated to monthly mean values at the 20º×20º model grid and averaged over 12 years. It is planed to extend the averaging period to 30 year in the next stage of the research.

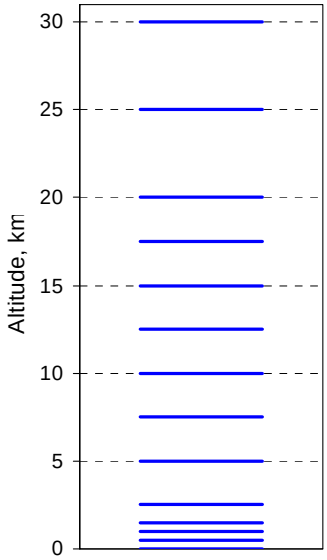

Fig. 22. *Vertical grid structure of the atmospheric model domain*

Mercury is presented in the atmosphere by two gaseous forms (elemental and oxidized), oxidized particulate form and aquatic forms in cloud water (dissolved elemental, mercury ion, sulfate and chloride complexes). Mercury fate in the atmosphere is determined by the following processes:

- Anthropogenic and natural emissions;
- Atmospheric dispersion;
- Chemical transformations in gaseous and aqueous phases;
- Dry deposition and wet scavenging.

Anthropogenic emissions data used in the study are described in Section 3.2. Natural emission and re-emission from land and the ocean are included into parameterization of appropriate air-surface exchange fluxes with soil and seawater and described below. Atmospheric dispersion is presented by simple upwind scheme with bi-directional fluxes between the gridboxes. The model utilizes completely the same chemical and wet deposition schemes as those in the full-scale model [*Travnikov and Ilyin*, 2005]. Dry deposition is described by simplified approach with fixed deposition velocities for different land-use types. Values of the dry deposition velocities were obtained by averaging appropriate velocities generated by the detailed dry deposition scheme of the full-scale model.

Ocean

The oceanic model domain covers open ocean and coastal waters as well as some inland seas (Baltic, Mediterranean, Black, Caspian, Red Seas, etc.) and consists of 6 irregular layers down to 1.2 km depth (Fig. 23). Oceanic processes are driven by sea currents and other data based on ECMWF ORA-S3 ocean re-analysis (http://www.ecmwf.int/products/forecasts/d/charts/ocean/) using averaging procedure similar to that for meteorological data described above.

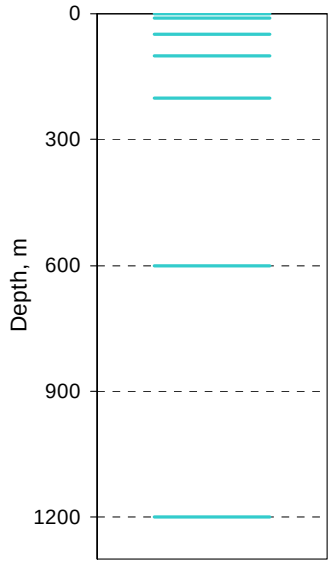

Fig. 23. *Vertical grid structure of the oceanic model domain*

Mercury in seawater is presented by three major forms – aqueous elemental, oxidized and non-reactive mercury [*Strode et al.*, 2007]. The model considers the following processes governing mercury fate in seawater:

- Dispersion with sea currents;
- Reduction of oxidized mercury to elemental form and conversion to non-reactive form;
- Gas exchange of dissolved elemental mercury with the atmosphere;
- Settling non-reactive mercury to the deep ocean with suspended particles.

Dispersion of mercury in the ocean is presented in the model using bi-directional flux scheme similar to that described above for the atmospheric transport. It accounts for oceanic transport of mercury with sea currents as well as upwelling and downwelling exchange with the deep ocean. In sea water mercury undergoes different biotic and abiotic transformations resulting in exchange between oxidized and elemental forms and conversion to non-reactive forms. Mechanisms and rate constants of these reactions are poorly known. Therefore, we applied a simplified description of these processes based on approach suggested by *S.A.Strode et al.* [2007].

The reaction rates for reduction of oxidized mercury and its conversion to the non-reactive form are assumed to be proportional to the ocean primary productivity of carbon and depend on solar radiation and depth of the ocean layer: $k_r = \alpha_r I_{pp} f(J_{solar}, z)$ *and* $k_c = \beta_c I_{pp} f(J_{solar}, z)$ for the reduction and

conversion, respectively. The reaction rates decreases with depth because of attenuation of solar radiation. Monthly mean fields of primary production [*Behrenfeld and Falkowski*, 1997] are available from (http://marine.rutgers.edu/opp). The rate constants α_r and β_c were constrained on available measurements of mercury concentration in seawater. Similar approach was applied to description of non-reactive mercury settling with particulate matter. Loss of mercury due to settling is determined by carbon flux estimated as primary productivity multiplied by the ratio ef of export to total production of carbon: $k_s = \gamma_s I_{pp} ef$. The temperature dependent ef ratio is taken from [*Laws et al*., 2000].

Air-sea exchange of dissolved elemental mercury is presented by the simple two layers model: $F_{ev} = k_w (C_{aq} - H_{Hg} C_g)$, where k_w is the gas exchange velocity and H_{Hg} is temperature dependent Henry's law constant for mercury. The empirical gas exchange velocity is a function of wind speed and the Schmidt number of considered substance [*Nightingale et al*., 2000].

Soil

Soil is presented in the model by one 20 cm depth layer. It is assumed that mercury occurs in soil in two forms – solid and dissolved in ground water. Solid form, in its turn, is divided into mercury content in mineral and organic soils. We expect that mercury in mineral soil has natural origin and is characterized by strong binding. Therefore, mineral mercury concentration is assumed to be constant (50 ng Hg/g) and non-zero only at the mercuriferrous belts location [*Gustin et al*., 1999]. On the contrary, mercury content in organic soils reflects accumulation of mercury mostly from atmospheric deposition and varies both spatially and temporally. Ground water concentration of mercury is related to the solid soil concentration by the soil-water partition coefficient $C_{dis} = C_{solid} / K_d$ [*Selin et al*., 2008; *Allison and Allison*, 2005]. The model considers the following processes governing mercury fate in soil:

- Evapotranspiration of ground water dissolved mercury to the atmosphere
- Run-off of ground water dissolved mercury to the ocean
- Volatilization of solid soil mercury to the atmosphere
- Prompt re-emission of newly deposited mercury

Evapotranspiration of moisture from land surface lead to loss of mercury to the atmosphere both directly from soil and through vegetation. Evapotranspirative flux of mercury can be estimated as a product of the water evapotranspiration rate and mercury concentration in soil water $F_{et} = I_{et} C_{dis}$ [*Selin et al*., 2008; *Xu et al.*, 1999]. Similar approach can be applied for evaluation of mercury loss due to run-off to the ocean $F_{ro} = I_{ro} C_{dis}$. Monthly mean estimates of soil water evapotranspiration and run-off rates [*Nijssen et al.,* 2001a; 2001b] are available from the VIC macroscale hydrologic model of the University of Washington (http://www.hydro.washington.edu/SurfaceWaterGroup/Data/vic_global.html).

Mercury volatilization flux from soil is described by the Arrhenius type equation $F_v = \varepsilon_v f(J_{solar}) C_{solid} \exp(-E_a/R_{univ}T_{soil})$ with empirically derived activation energy E_a taken from literature [*Kim et al*., 1995; *Capri and Lindberg*, 1998; *Poissant and Casimir*, 1998]. The pre-exponetial factor is a function of solid soil mercury concentration and solar radiation. Dependence of mercury volatilization flux on soil moisture did not considered in this study.

A number of isotopic studies [e.g. *Hintelmann et al.*, 2002; *Amyot et al*., 2004] have demonstrated that newly deposited mercury is more available for re-emission than strongly bound indigenous mercury. Following *N.E.Selin et al*. [2008] we adopted prompt re-emission of 20% atmospheric deposition to soil and vegetation and 60% of deposition to snow cover.

Historical emissions

An important type of input information required for estimates of mercury cycling and long-term accumulation in the environment is historical emissions. Up to date, there is no reliable estimates of mercury anthropogenic emission changes since pre-industrial period till nowadays. For the research purpose, we performed rough estimates of historical emission trend of mercury using approach suggested by *R.J.M. Hudson et al.* [1995]. Modern anthropogenic emissions were taken from the recent global mercury emission inventory for 2005 [*AMAP/UNEP*, 2008]. Since much of global mercury emission is originated from coal and other fuels combustion [*AMAP/UNEP*, 2008] we approximated historical evolution of mercury emission by scaling modern emission levels by a factor derived from historical trend of CO_2 emissions from fossil fuel combustion. Global data on fossil-fuel CO_2 emissions [*Andres et al*., 1999] are available from the Carbon Dioxide Information Analysis Centre (http://cdiac.ornl.gov/trends/emis/overview.html).

It is clear that this trend does not reflect historical evolution of mercury emissions from other important sources including metal and cement production, waste incineration and artisanal gold mining. Therefore, in order to estimate the effect of one of the most important historical mercury emission episodes on mercury cycling in the environment we also considered emission of the pollutant from gold and silver mining in North America (Fig. 24.). According to different estimates annual emission of mercury from this source in the second half of 19th century could be of the same order or comparable with modern global mercury emission [*Hudson et al.,* 1995, *Strode et al.*, 2009]. To evaluate contribution of this source we used recent estimates of mercury emission from North American gold rush in 1870-1880 by *S.Strode et al.* [2009] and primary mercury production in North America [*Hylander and Meili*, 2003] as the temporal scaling factor.

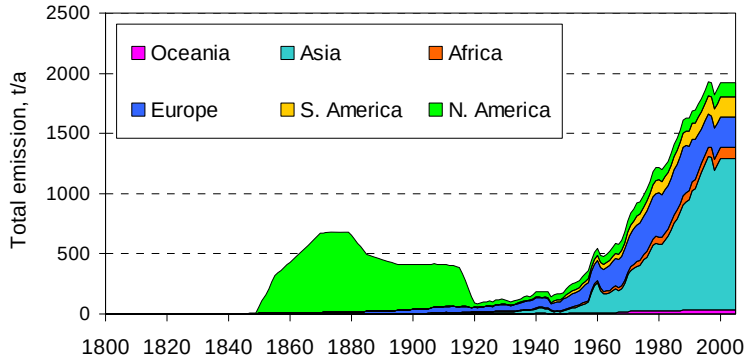

Fig. 24. *Estimated historical emissions of mercury from fossil fuel combustion as well as gold and silver mining in North America*

Simulation of Hg cycling in the environment

Pre-industrial conditions were simulated by reaching steady-state with zero anthropogenic emissions. After that we performed 200 years simulation from the beginning of 19th century to nowadays using historical anthropogenic emissions discussed above. Figure 25a shows simulated changes of total mercury burden in the atmosphere, soil and the ocean as well as atmospheric deposition. The signal of mercury emission from North American gold and silver mining is clearly seen in the atmospheric mass and deposition. Response of the ocean was significantly smaller and almost no effect was obtained for the soil burden. The total mercury burden in the atmosphere has increased more then twice since the pre-industrial period till nowadays, mercury in the ocean – by about 25%, and about

10% increase was obtained for mercury in soil. It should be noted, that increase of mercury concentrations in the upper layers of soil and the ocean is more significant than in the whole media and can reach a factor of two. The largest enrichment due to anthropogenic activity was obtained for atmospheric deposition: it was enlarged by a factor 2.3. Besides, the deposition increase varies between different regions and continents (Fig. 25b). For example, in Asia it exceeds a factor of 3 whereas is South America it is smaller then a factor of 2.

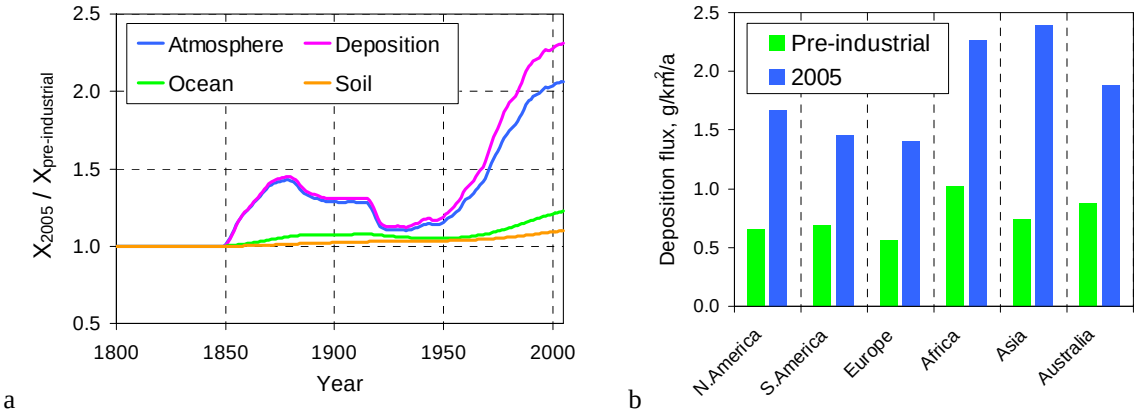

Fig. 25. *Simulated evolution of total mercury burden in three main environmental media and atmospheric deposition since 1800 till 2005 (a) and increase of average deposition flux in different continents (b)*

Figure 26 shows spatial distribution of simulated present-day concentrations of mercury in the atmosphere, soil and the ocean as well as wet deposition flux. For comparison, limited number of mercury measurements in different media are also presented in the figure. As seen modelled gaseous elemental mercury in general reproduce the observed values, particularly, in the Northern Hemispher but somewhat underestimate south-to-north gradient (Fig. 26a). Wet deposition pattern mainly reflects combination of three factors: location of major anthropogenic source regions, distribution of precipitation and spatial pattern of major oxidants concentration affecting mercury oxidation and removal. There is some overestimation of observed wet deposition fluxes in North America and Europe. Concentrations of dissolved elemental mercury in seawater are high in regions with significant upwelling and primary productivity of carbon where reduction of oxidized form is more efficient (Fig. 26c). Elevated concentrations of mercury in soil, in general, follow location of major mercuriferrous belts (western coast of Americas and eastern coast of Eurasia) and regions with significant anthropogenic emissions (Fig. 26d). In the first case, they reflect naturally mercury enriched areas, whereas in the second case high concentrations result from accumulation of atmospheric deposition.

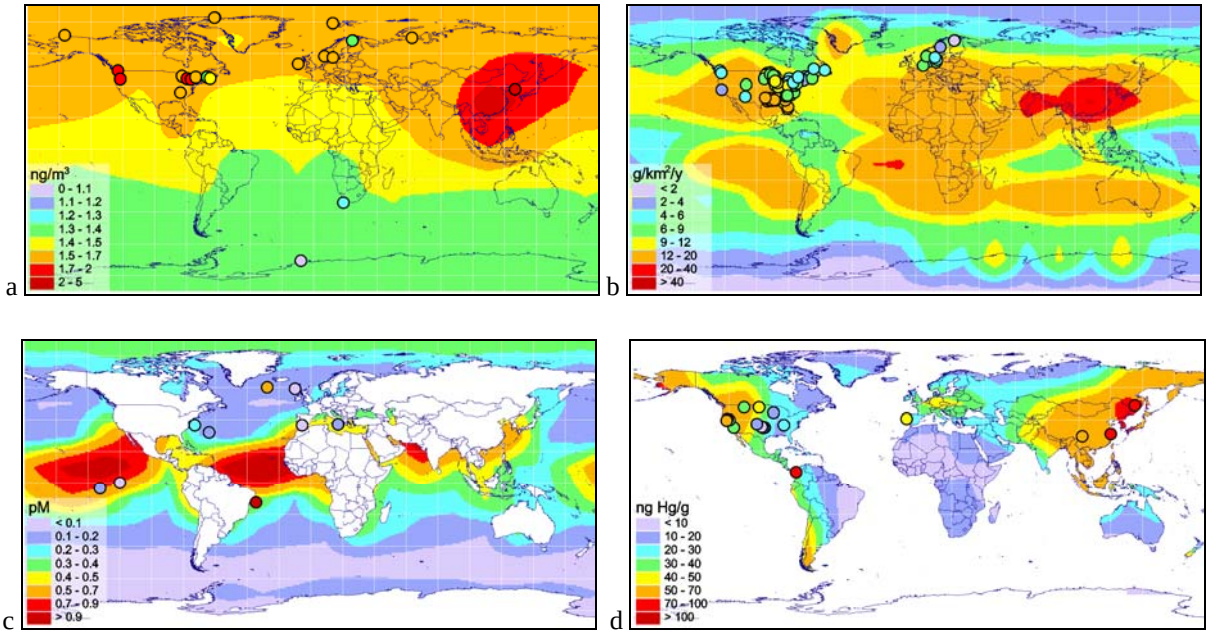

***Fig. 26**. Simulated present-day concentration of elemental gaseous mercury in ambient air (a), mercury wet deposition flux (b), concentration of dissolved elemental mercury in seawater (c) and mercury concentration in soil (d). Circles present long-term measurements data available from literature.*

In order to investigate long-term media response to changes of anthropogenic emissions we performed simulation of two artificial future scenarios. The first one – *cut-off scenario* – simulates recovering of the global environment in case when global anthropogenic emissions are completely stopped (Fig. 27a). As seen from the figure, total atmospheric burden and deposition of mercury decreases quickly during the first 10 years. After that the decrease is slowing down when the atmosphere reaches equilibrium with soil which changes very slowly remaining somewhat enriched with mercury in comparison with pre-industrial period. The ocean burden of mercury gradually decreases during the next a hundred years. The second – *status quo scenario* – considers changes of mercury levels in the environment if the current emissions are fixed in future. In this case the model predicts further growth of mercury levels in all media (Fig. 27b).

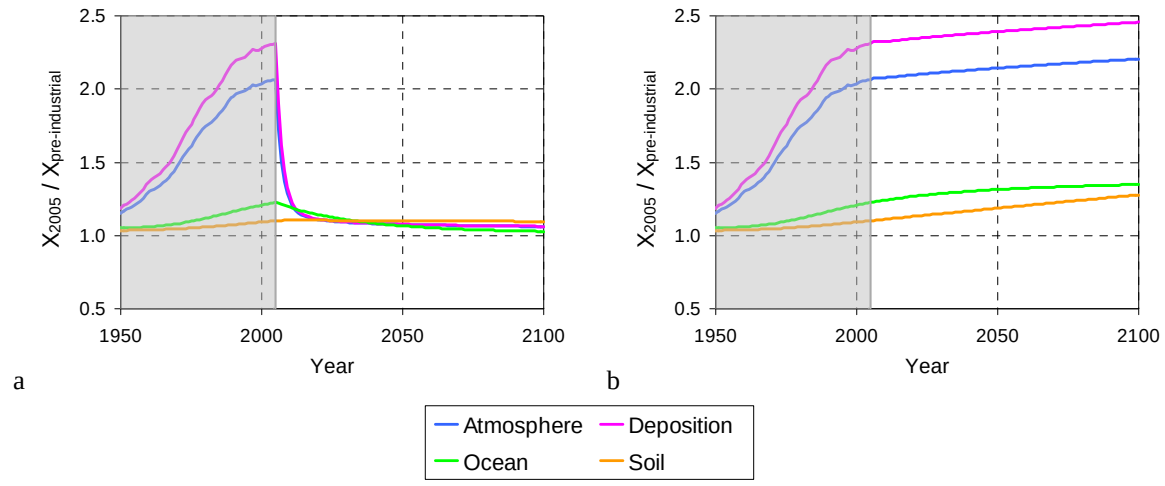

***Fig. 27.** Simulated evolution of total mercury burden in three main environmental media and atmospheric deposition for two artificial future scenarios: "cut-off" scenario (a) and "status quo" scenario (b)*

FUTURE ACTIVITY

In accordance with the EMEP workplan for 2010 [ECE/EB.AIR/GE.1/2009/13], the activities of the EMEP Centres for the next year in the field of the global scale modelling include three major aspects – improvements of emission inventories on a global scale, further development of the common EMEP global modelling framework and close co-operation with Task Force on Hemispheric Transport of Air Pollution.

Improvement of emission inventories on a global scale:

- evaluate the new EDGAR HTAP global emission data in comparison with other available expert estimates (CEIP, MSC-W, MSC-E); this task will be performed within the framework of the TF HTAP taking part in the planned model intercomparison (see below);

Further development of the common EMEP global modelling framework:

- evaluate the effect of using different geophysical and emission data in the existing global models used at the two Meteorological Synthesizing Centres (MSC-W, MSC-E);

- evaluate means for the flexible introduction of different meteorological drivers to be used in the common EMEP global model (MSC-E, MSC-W);

- identify the changes in existing model routines that are necessary to facilitate common modules for global modelling in EMEP (MSC-W, MSC-E);

Co-operation with TF HTAP:

- Participate in the TF HTAP model intercomparison for ozone, PM compounds, POPs and heavy metals with the two EMEP global models (MSC-W, MSC-E);

- Contribute to the TF HTAP 2010 assessment report on intercontinental transport of air pollution (MSC-E, MSC-W, CIAM, CCC).

REFERENCES

Allison J.D. and Allison T.L. [2005] Partition coefficients for metals in surface water, soil and waste. Rep.EPA/600/R-05/074, U.S. Environ. Prot. Agency, Off. Of Res. And Dev., Washington, D.C.

AMAP/UNEP [2008] Technical background report to the global atmospheric mercury assessment. Arctic Monitoring and Assessment Programme / UNEP Chemicals Branch. 159 pp. (available at http://www.chem.unep.ch/mercury/).

Amyot M., Southworth G., Lindberg S.E., Hintelmann H., Lanlonde J.D., Orgrinc N., Poulain A.J., Sandilands K.A. [2004] Formation and evasion of dissolved gaseous mercury in large enclosures amended with $^{200}HgCl2$. *Atmos. Environ.* 38, 4279–4289.

Andres R.J., D.J. Fielding, G. Marland, T.A. Boden, and N. Kumar [1999] Carbon dioxide emissions from fossil-fuel use, 1751-1950. *Tellus* 51B, 759-65.

Behrenfeld M.J. and Falkowski P.G. [1997] Photosynthetic derived from satellite-based chlorophyll concentration. *Limnol. Oceanogr*., 42(1), 1-20.

Berglen T. F., T. K. Bernsten, I. S. A. Isaksen, and J. K. Sundet [2004] A global model of the coupled sulfur/oxidant chemistry in the troposphere: The sulfur cycle. *J. Geophys. Res*., 109, doi:10.1029/2003JD003948.

Boersma K.F., H.J. Eskes, E.J. Brinksma [2004] Error analysis for tropospheric NO2 retrieval from space. *J. Geophys. Res.*, 109, doi:10.1029/2003JD003962.

Carmichael G.R., T. Sakurai, D. Streets, Y. Hozumi, H. Ueda, S.U. Park, C. Fung, Z. Han, M. Kajino,, M. Engardt, C. Bennet,, H. Hayami, K. Sartelet, T. Holloway, Z. Wang, A. Kannari, J. Fu, K. Matsuda, N. Thongboonchoo and M. Amann [2008] MICS-Asia II: The model intercomparison study for Asia Phase II methodology and overview of findings. *Atm. Env*., 42 pp 3468–3490.

Carpi A. and Lindberg S. E. [1998] Application of a teflonTM dynamic flux chamber for quantifying soil mercury flux: tests and results over background soil. *Atmos. Environ.* 32(5), 873-882.

Fagerli, H., P. Wind, M. Gauss, Á. Nyíri, D. Simpson and S. Tsyro. [2008], Improved resolution in EMEP models In: *Transboundary acidification, eutrophication and ground level ozone in Europe in 2006*, EMEP/MSC-W Status. Rep. 1/2008 The Norwegian Meteorological Institute, Oslo, Norway

Gusev A., Mantseva E., Shatalov V., Travnikov O. [2005] Hemispheric model (MSCE-Hem) of persistent toxic substances dispersion in the environment. MSC-E Technical Report 11/2005, Meteorological Synthesizing Centre East of EMEP, Moscow (available at http://www.msceast.org/publications.html).

Gustin M.S., Lindberg S., Marsik F., Casimir A., Ebinghaus R., Edwards G., Hubble-Fitzgerald C., Kemp R., Kock H., Leonard T., London J., Majewski M., Montecinos C., Owens J., Pilote M., Poissant L., Rasmussen P., Schaedlich F., Schneeberger D., Schroeder W., Sommar J., Turner R., Vette A., Wallschlaeger D., Xiao Z., and Zhang H. [1999] Nevada STORMS project: Measurement of mercury emissions from naturally enriched surfaces. *J. Geophys. Res*. 104(D17), 21831-21844.

Hintelmann H., St. Louis V., Scott K., Rudd J.W.M., Lindberg S.E., Krabbenhoft D., Kelly C., Heyes A., Harris R., Hurley J. [2002] Reactivity and mobility of newly deposited mercury in a Boreal catchment. *Environ. Sci. Technol.* 36, 5034–5040.

Hudson R.J.M., Gherini S.A., Fitzgerald W.F., Porcella D.B. [1995] Anthropogenic influences on the global mercury cycle: a model-based analysis. *Water, Air, and Soil Pollution* 80, 265-272 .

Hylander L.D., Meili M. [2003] 500 years of mercury production: global annual inventory by region until 2000 and associated emissions. *Science of the Total Environment* 304, 13–27.

Jonson J.E., L. Tarasón, P. Wind, M. Gauss, S. Valiyaveetil, S. Tsyro, H. Klein, I.S.A. Isaksen and A. Benedictow [2007] First evaluation of the global EMEP model and comparison with the global OsloCTM2 model EMEP/MSC-W Tech. Rep. 2/2007The Norwegian Meteorological Institute, Oslo, Norway.

Kim K.-H., Lindberg S. E. and Meyers T. P. [1995] Micrometeorological measurements of mercury vapor fluxes over background forest souls in eastern Tennessee. *Atmos. Environ.* 29(2), 267-282.

Laws E.A., Falkowski P.G., Smith W.O. Jr., Ducklow H., McCarthy J.J. [2000] Temperature effects on export production in the open ocean. Global Biogeochemical Cycles 14, 1231-1246.

Mason R. P. [2009] Mercury emissions from natural sources and their importance in the global mercury cycle. In: Mercury Fate and Transport in the Global Atmosphere: Emissions, Measurements and Models (eds. N. Pirrone and R. Mason), Springer, USA.

Michalakes J., J. Dudhia, D. Gill, T. Henderson, J. Klemp, W. Skamarock, and W. Wang [2004] The Weather Reseach and Forecast Model: software architecture and performance. In: Zwiefhofer W., Mozdzynski G.

(Eds.), Proceedings of the Eleventh ECMWF Workshop on the Use of High Performance Computing In Meteorology. World Scientiic, pp.156-168

Nightingale P.D., Malin G., Law C.S., Watson A.J., Liss P.S., Liddicoat M.I., Boutin J., Upstill-Goddard R.C. [2000] In situ evaluation of air-sea gas exchange parameterizations using novel conservative and volatile tracers. *Global Biogeochemical Cycles* 14, 373-387.

Nijssen B., Schnur R., and Lettenmaier D.P. [2001a] Global Retrospective Estimation of Soil Moisture Using the Variable Infiltration Capacity Land Surface Model, 1980-93, *Journal of Climate*, 14, 1790-1808.

Nijssen B., O'Donnell G., Lettenmaier D.P., Lohmann D., and Wood E.F. [2001b] Predicting the Discharge of Global Rivers, *Journal of Climate,* 14, 3307–3323.

Poissant L. and Casimir A. [1998] Water–air and soil–air exchange rate of total gaseous mercury measured at background sites. *Atmos. Environ.* 32(5), 883-893.

Selin N.E., Jacob D.J., Yantosca R.M., Strode S., Jaeglé L., Sunderland E.M. [2008] Global 3-D land-ocean-atmosphere model for mercury: Present-day versus preindustrial cycles and anthropogenic enrichment factors for deposition. *Global Biogeochemical Cycles* 22, GB2011.

Skamarock, W. C., J. B. Klemp, J. Dudhia, D. O. Gill, D. M. Barker, W. Wang and J. G. Powers [2005] A Description of the Advanced Research WRF Version 2. NCAR Technical note NCAR/TN-468

Streets D., T. Bond, G. Carmichael, S. Fernandes, Q. Fu, D. He, Z. Klimont S. Nelson, N. Tsai, M. Wang, J.-H. Woo and K. Yarber [2003] An inventory of of gaseous aerosol emissions Asia in the year 2000. *J. Geophys. Res.,* 108, doi:10.1029/2002JD003093.

Strode S., Jaeglé L., Selin N.E. [2009] Impact of mercury emissions from historic gold and silver mining: Global modelling. *Atmos. Environ.* 43(12), 2012-2017.

Strode S.A., Jaeglé L., Selin N., Jacob D., Park R.J., Yantosca R.M., Mason R.P., Slemr F. [2007] Air-sea exchange in the global mercury cycle. *Global Biogeochemical Cycles* 21, GB1017.

Tarrasón L. and A. Gusev Ed. [2008] Towards the development of a common EMEP global modelling framework EMEP/MSC-W Technical Report 1/2008

Tiedke M. [1989] A comprehensive mass flux scheme for cumulus parameterization on large scale models. *Mon. Weather Rev*., 117:1,779-1, 800.

Travnikov O. and I.Ilyin [2005] Regional Model MSCE-HM of Heavy Metal Transboundary Air Pollution in Europe. EMEP/MSC-E Technical Report 6/2005, 59 pp. (available at http://www.msceast.org/publications.html).

Xu X.H., Yang X.S., Miller D.R., Helble J.J., and Carley R.J. [1999] Formulation of bi-directional atmosphere-surface exchanges of elemental mercury. *Atmos. Environ.*, 33(27), 4345– 4355.